Battle of the Backbones: A Large-Scale Comparison of Pretrained Models across Computer Vision Tasks

Micah Goldblum[1] *   **Hossein Souri**[2] *   **Renkun Ni**[3]   **Manli Shu**[3]   **Viraj Prabhu**[4]

Gowthami Somepalli[3]   **Prithvijit Chattopadhyay**[4]   **Mark Ibrahim**[6]   **Adrien Bardes**[5,6]

Judy Hoffman[4]   **Rama Chellappa**[2]   **Andrew Gordon Wilson**[1]   **Tom Goldstein**[3]

Abstract

Neural network based computer vision systems are typically built on a *backbone*, a pretrained or randomly initialized feature extractor. Several years ago, the default option was an ImageNet-trained convolutional neural network. However, the recent past has seen the emergence of countless backbones pretrained using various algorithms and datasets. While this abundance of choice has led to performance increases for a range of systems, it is difficult for practitioners to make informed decisions about which backbone to choose. Battle of the Backbones (BoB) makes this choice easier by benchmarking a diverse suite of pretrained models, including vision-language models, those trained via self-supervised learning, and the Stable Diffusion backbone, across a diverse set of computer vision tasks ranging from classification to object detection to OOD generalization and more. Furthermore, BoB sheds light on promising directions for the research community to advance computer vision by illuminating strengths and weakness of existing approaches through a comprehensive analysis conducted on more than 1500 training runs. While vision transformers (ViTs) and self-supervised learning (SSL) are increasingly popular, we find that convolutional neural networks pretrained in a supervised fashion on large training sets still perform best on most tasks among the models we consider. Moreover, in apples-to-apples comparisons on the same architectures and similarly sized pretraining datasets, we find that SSL backbones are highly competitive, indicating that future works should perform SSL pretraining with advanced architectures and larger pretraining datasets. We release the raw results of our experiments along with code that allows researchers to put their own backbones through the gauntlet here: https://github.com/hsouri/Battle-of-the-Backbones.

1   Introduction

The dominant paradigm for building machine vision systems involves a feature extractor network, also known as a *backbone*, which feeds into a task-specific *head*. The backbone might output a dense array of features for object detection and localization, or a single feature vector for classification or image retrieval. While backbones can be trained from scratch on task-specific data, many off-the-shelf backbones are pretrained on large benchmark datasets and then fine-tuned for the task at hand. This transfer learning approach has several advantages. First, it dramatically reduces the application-specific data requirements of deep learning and has led to improved performance on a wide range of

---

https://doi.org/10.52202/075280-1277

applications. Second, it can speed up training and reduce compute costs even when large amounts of task-specific data are available [29]. Finally, pretraining datasets often contain images from many disparate domains, resulting in model robustness that can be transferred to downstream tasks.

Early deep learning based vision systems relied heavily on ImageNet pretraining [23, 59]. In contrast, today's practitioners have access to a cornucopia of choices, with different pretrained models resulting in significant performance differences. There are three primary factors that influence the performance of such a model: its architecture, the pretraining algorithm, and the pretraining dataset. Each of these design dimensions presents many options, resulting in a dizzying array of choices for practitioners building a computer vision system. Despite this wide variety of choices, practitioners have no resource to turn to and instead are left piecing together results from method papers or testing out the backbones themselves.

We pit these backbones against each other in a *Battle of the Backbones* (BoB). BoB compares many popular publicly available pretrained checkpoints, as well as randomly initialized baselines, on a wide variety of downstream tasks including image classification on natural, medical, and satellite images (Section 3.1), object detection and segmentation (Section 3.2), out-of-distribution generalization (Section 3.3), and image retrieval (Section 3.4).

Aside from assisting practitioners building computer vision systems, another central goal of this benchmark is to help guide the research community towards fruitful research directions in their quest for designing better backbones. BoB sheds light on the strengths and weaknesses of pretraining routines and architectures, revealing popular misconceptions and fundamental limitations, as well as promising directions for improvement. Below, we summarize several of our primary findings and discuss previous efforts for comparing backbones.

1.1 Battle of the Backbones: The TLDR

The subsequent sections in this paper contain numerous experimental details. Therefore, we distill several key findings below:

▷ Across the suite of comprehensive evaluations in BoB, spanning tasks, datasets, and settings (including ID and OOD), supervised ConvNeXt-Base, supervised SwinV2-Base trained using ImageNet-21k, and CLIP ViT-Base come out on top. The same winners also win at smaller scales. Among smaller backbones, ConvNeXt-Tiny and SwinV2-Tiny emerge victorious, followed by DINO ViT-Small.
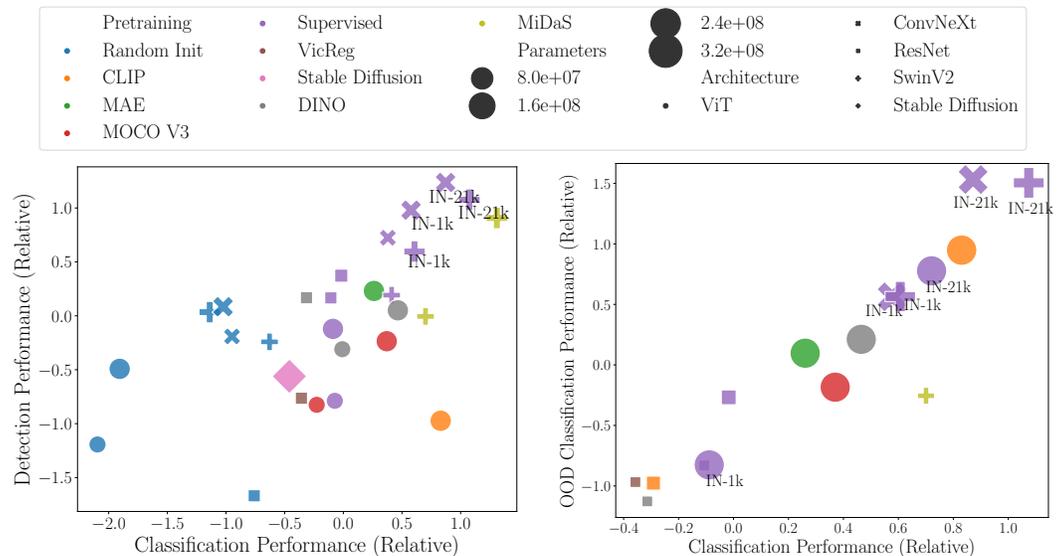

Figure 1: **Performance is correlated across tasks.** Performance for each model is reported in terms of standard deviations above/below the mean averages across datasets. **Left:** Comparison between classification and detection. **Right:** Comparison between classification and OOD classification.

▷ Despite the recent attention paid to transformer-based architectures and self-supervised learning, high-performance convolutional networks pretrained via supervised learning outperform transformers on the majority of tasks we consider.

▷ The observed superiority of supervised pretraining occurs because such models are often trained on larger datasets. In apples-to-apples comparisons on the same dataset scale, SSL models outperform their supervised counterparts.

▷ ViTs are more sensitive to the amount of pretraining data and the number of parameters than CNNs.

▷ Performance across tasks is strongly correlated – the top-performing backbones in BoB tend to be universally good across tasks and settings. See Figure 1.

1.2 Previous Benchmarks

Throughout much of the last decade, the most popular backbones were pretrained on ImageNet [17]. Since 2020, SimCLR [10] and CLIP [73] have popularized self-supervised backbones and spawned much new research. While method papers that propose a new pretraining routine typically compare to similar competitors on several downstream tasks, we focus in this section on works that specifically benchmark large collections of backbones on diverse tasks.

In 2019, Goyal et al. [25] compared AlexNet [47] and ResNet-50 [28] models pretrained using `colorization` and `jigsaw` pretext tasks to supervised learning models, finding that supervised learning massively outperformed SSL at the time. Kolesnikov et al. [44] similarly compared several pretext tasks and convolutional neural network architectures, showing that architectural advances on supervised learning do not always translate to improved self-supervised learning. Kornblith et al. [45] instead benchmarked the transferability of ImageNet-trained supervised learning models on downstream classification tasks, varying the architecture and finding that the correlation between downstream performance and ImageNet test accuracy is nearly perfect across architectures. In the same year, Zhai et al. [107] built the Visual Task Adaptation Benchmark (VTAB) and tested various self-supervised learning methods including VAEs and GAN discriminators, also exhibiting the dominant performance of supervised learning models. In 2020, Ericsson et al. [21] evaluated ResNet-50 models trained on ImageNet using various SSL algorithms, finding that the performance of then-existing SSL algorithms on a richer set of downstream tasks were strongly correlated with their ImageNet-1k test accuracy and finding improved performance of the newer SSL algorithms compared to previous studies.

Since the above works, pretraining algorithms along with their training sets and architectures have made tremendous progress, and whereas supervised learning was previously the default approach to pretraining, the options now are endless. Therefore, benchmarking backbones deserves renewed attention. See Appendix A for an additional survey of task-specific benchmarks.

2 A Guide to BoB

Among the distinguishing features of the diverse backbones competing in our battle are their architectures, pretraining routines, and the datasets on which they were pretrained. Table 1 contains an overview of the backbones we benchmark including their pretraining algorithms, pretraining datasets, and architectures. We also provide a more detailed description of these features and the precise pretrained checkpoints we use in Appendix B.

A Note on Scale and Apples-to-Apples Comparison. *Many practitioners have limited compute and moreover will need to tune hyperparameters on their own datasets without exceeding their compute budget. To simulate this scenario, we perform moderate hyperparameter sweeps, we preclude particularly long training schedules, and we do not consider architectures bigger than ConvNeXt-Base, except for the Stable Diffusion backbone which does not come in a smaller size. Specific hyperparameter grids are detailed in subsequent sections. Moreover, we only use publicly available checkpoints that would also be accessible to practitioners. Available checkpoints were pretrained with varying amounts of hyperparameter tuning, and different pretraining algorithms were trained on different datasets and architectures making a precise apples-to-apples comparison infeasible. Nevertheless, this comparison of existing checkpoints is the relevant one for practitioners, as it represents realistic conditions, and we use identically sized hyperparameter sweeps for each backbone on downstream tasks.*

Table 1: **A synopsis of the backbones we benchmark.** Columns correspond to the pretraining algorithm, a coarse categorization, the pretraining dataset, and the architectures we include. A detailed description of each algorithm, pretraining dataset, and architecture can be found in Appendix B.

Pretraining	Style	Dataset	Architecture(s)
MoCo v3 [12]	SSL	ImageNet-1k [17]	ViT [18]
VICReg [3]	SSL	ImageNet-1k	ResNet [28]
VICRegL [4]	SSL	ImageNet-21k	ConvNeXt [58]
DINO [8]	SSL	ImageNet-1k	ResNet, ViT
MAE [30]	SSL	ImageNet-1k	ViT
Stable Diffusion [77]	Vision-Language	LAION-2B [81]	Stable Diffusion encoder
CLIP [73]	Vision-Language	LAION-2B, CLIP	ResNet, ViT
MiDaS [75]	Supervised	$12 \times$ Depth Datasets	SwinV2 [57]
Image classification	Supervised	ImageNet-21k,-1k	All above architectures
Random initialization	None	N/A	All above architectures

2.1 The Tasks

In order to comprehensively probe the capabilities of the backbones, we evaluate their performance both fine-tuned and frozen on a number of downstream tasks belonging to the following categories:

- **Classification:** We measure both fine-tuned and linear probe performance of backbones on various downstream classification tasks including natural, medical, or satellite image datasets in Section 3.1. Image classification tasks require that a backbone extract features which identify the content of an image's foreground but not necessarily how many of an object there are or where they are located within an image.

- **Object detection and segmentation:** Unlike image classification, dense prediction tasks require backbones to extract features containing the precise locations of objects, on a pixel basis for segmentation and in enough fidelity to draw bounding boxes for object detection. We evaluate backbones on both of these tasks in Section 3.2.

- **Out-of-distribution generalization:** In real-world applications, computer vision systems are often deployed on data which does not reflect their training set distribution. Even high-performing models are known to fail under domain shifts [71, 32]. Therefore, we evaluate the abilities of models both to generalize to new downstream domains in Section 3.3.

- **Image retrieval:** Image retrieval requires a backbone to match like images via proximity in feature space. We explore tasks that require matching the images with respect to various criteria such as semantic content and visual similarity in Section 3.4.

3 Experimental Setup

We now describe our experimental setup for each task. Specifically, we list learning protocols, datasets, and evaluation metrics. Find complete experimental and implementation details in Appendix C.

3.1 Classification

Learning protocols. We evaluate pretrained backbones on various datasets under two fine-tuning protocols, following previous works [12, 30, 8, 10]: **end-to-end fine-tuning** (including experiments with only a small number of labeled samples) and **linear probing**. In the former scenario, we fine-tune the full model end-to-end on a given dataset or on a fraction of it, and we measure the accuracy on the test split. In the linear probing scenario, we extract features from the frozen pretrained backbone, and only learn a linear classifier on top of these pretrained representations. These two protocols are widely used in previous work to evaluate the quality of pretraining methods such as in self-supervised learning [12, 30, 8, 10] and vision-language pretraining [1, 106].

Datasets and evaluation metrics. We conduct experiments on 6 common image classification datasets, covering multiple domains such as natural images (ImageNet-1K [17], CIFAR-100 [46],

Flowers-102 [65], Aircraft [61]), satellite images (EuroSAT [31]), and medical X-ray data (CheXpert [37]) showing the generalization and transferability of the pretrained backbones. All datasets we use are publicly available, and we list their details including size and the number of classes in Appendix C. For experiments with only a fraction of the training set, we randomly sample 1% and 10% of the training samples and fine-tune the pretrained backbones on these subsets. When sampling the subsets, we maintain the original dataset's label distribution. Note that we only consider in-domain generalization here, where the training and testing splits are from the same source.

To evaluate, we measure *classification accuracy* and *Area Under the ROC Curve* (AUC) on the test split as performance metrics for single-label and muti-label classification tasks, respectively. In addition to the best score among hyperparameter vectors, we also plot the accuracy for the first several epochs to show the convergence rate of different pretrained backbones. Moreover, we benchmark the latency and the memory usage of each backbone on the same device.

3.2 Object Detection and Segmentation

Learning protocols. For evaluations on object detection and instance segmentation, we employ the Cascade Mask R-CNN framework [5]. We conduct experiments with three protocols: **(1)** end-to-end training from random initialization, **(2)** end-to-end finetuning using pretrained backbones, and **(3)** finetuning with frozen backbones. Whereas finetuning with a frozen backbone is atypical in segmentation and detection, this latter protocol allows us to probe localization within features extracted by pretrained models and complements linear probing classification experiments. See Appendix C.1 for a discussion on the potential for ViTs, especially large ones, to exceed the performance of other models under more expensive training protocols.

Datasets and evaluation metrics. We conduct object detection and instance segmentation evaluations on the popular COCO dataset [54]. We follow the COCO-style average precision (AP) metric, which calculates the average across various Intersection over Union (IoU) thresholds. We report the box Average Precision (box AP), box AP@50, and AP@75 for object detection and mask Average Precision (mask AP), mask AP@50, and mask AP@75 for instance segmentation [55].

3.3 Out-of-Distribution Generalization

While modern networks may exhibit strong performance on data distributions they are trained on, a wide body of prior work [71, 32] has found that the performance of such models can degrade significantly under distribution shifts. In addition to evaluating the in-distribution performance of backbones across a diverse set of downstream tasks, we also consider how this performance translates to out-of-distribution (OOD) settings.

Learning protocols. Several task-specific datasets and benchmarks have been proposed to evaluate the robustness of models to deviations from their training distributions. Concretely, we study the generalization of the trained backbones on two tasks, **(1)** image classification and **(2)** object detection, and on two types of distribution shifts, **(A)** structure and style variations within ImageNet and **(B)** synthetic-to-real generalization.

Datasets and evaluation metrics. We consider the following broad benchmarks for OOD evaluation:

(A) Robustness to changes in structure and style. We measure OOD generalization of ImageNet-trained or fine-tuned models on the following benchmarks: **(i)** ImageNet-A [34]. ImageNet-A(dversarial) contains a curated subset of ImageNet test images spanning 200 categories that are especially challenging for trained deep models. **(ii)** ImageNet-V2 [76]. ImageNet-V2 is an additional test set of ImageNet-like images collected a decade after the original dataset following an identical collection protocol. **(iii)** ImageNet-R [33]. ImageNet-R(endition) contains artistic renditions for 200 categories from ImageNet, including cartoons, graffiti, embroidery, origami, sculptures, *etc.* **(iv)** ImageNet-S [93]. ImageNet-S(ketch) is a web-crawled and manually cleaned collection of black and white sketch images from ImageNet categories.

(B) Syn-to-real generalization. We also measure the performance of models trained on synthetic data and tested on real data. Synthetic data has emerged as a popular alternative in settings where it may be hard or expensive to curate reliably annotated real-world data. We measure syn-to-real generalization for image classification and object detection on the two following popular benchmarks: **(i)** VisDA Syn→Real. The VisDA classification benchmark consists of $\sim$ 152k synthetic images and

$\sim$ 55k real images across 12 classes. The synthetic images in VisDA are 3D renderings of objects from multiple viewpoints and under different lighting conditions. The real counterparts are crops of the 12 classes obtained from the COCO dataset. **(2)** Sim10k→Cityscapes. For object detection, we use Sim10k as the synthetic training dataset and Cityscapes as the real evaluation dataset. Sim10k consists of $\sim$ 10k street view images (drawn from GTAV). Cityscapes consists of $\sim$ 5k densely annotated street view images curated from vehicular viewpoints in the real world. Following prior work [13], we train on the entirety of Sim10k to detect instances of "car" and measure detection performance on the validation split of Cityscapes.

We report generalization performance using classification accuracy on the OOD test set for image classification and mean average precision or mAP@50 for object detection.

3.4   Image Retrieval

We conduct evaluations on a diverse set of retrieval datasets encompassing content-based image retrieval and classification datasets that we repurpose for semantic retrieval tasks. For geographic landmark retrieval, we utilize the Oxford dataset [69] and the Paris dataset [70]. To ensure accuracy, we employ the cleaned-up versions of these datasets with corrected labels [72]. The INSTRE dataset [95] consists of objects such as toys and irregularly-shaped products placed in different locations and conditions. To examine fine-grained retrieval, we employ the Caltech-UCSD Birds-200 dataset (CUB-200) [91], which contains various bird classes captured under different backgrounds, poses, and lighting conditions. For a diverse set of natural images, we use the iNaturalist dataset [88]. This dataset offers a wide range of fine-grained categories classified into 13 super-categories, including Plant, Insect, Bird, and Mammal. To evaluate retrieval performance in real-world scenarios, we employ the Objectnet dataset [2]. This dataset consists of 313 object classes with randomly varying backgrounds, rotations, and imaging viewpoints. For large-scale landmark recognition, we utilize the Google Landmarks v2 dataset [99], which includes approximately 200,000 unique landmarks. Lastly, we employ the INRIA Copydays dataset [19], which comprises a small collection of holiday photos. Among the datasets mentioned, iNaturalist, Objectnet, and CUB-200 can be categorized as semantic retrieval datasets, while the remaining datasets fall under content-based retrieval datasets.

To evaluate, we measure model performance using mean-Average-Precision or *mAP* [68]. We first compute the average precision for a given query image, and then compute the mean over all queries to find the mAP. We also measure *Recall@k*, which measures the proportion of correct matches among the top k, and *MRR* (Mean Reciprocal Rank), which records the number of results returned before the first correct match and computes the mean of the reciprocal of these misses. Higher is better for all metrics.

4   I'm a Practitioner. Which Backbone Should I Choose?

Practitioners today can choose from a large catalogue of backbones of varying sizes, training methods, and pretraining data: which backbone should a practitioner select for a particular task or in general? To answer this question, in BoB, we systematically compare publicly available backbones (see Table 1) across multiple tasks, datasets and settings. To make these comparisons, we use the following ranking protocol:

(1) Setting-specific Z-Scores. For a particular task and setting (e.g, top-1 classification accuracy on ImageNet), we first compute z-scores for all the backbones being evaluated – i.e., for setting specific performance (e.g., accuracy) values $\{x_i\}_{i=1}^N$, z-scores are computed as $\{\frac{x_i-\mu}{\sigma}\}_{i=1}^N$ where μ and σ are the mean and standard deviation of the sample. This allows us to measure how good a specific backbone is (stds above or below) compared to "mean" performance of all backbones in that setting.

(2) Cross-setting Comparisons. To compare backbones across different tasks and settings, we simply aggregate and compare the previously obtained z-scores to obtain a relatively (coarse) ranking of backbones.

Using rankings, we can report not only the best performing backbones for each task but also the best backbone in terms of overall performance across tasks, datasets and settings (see Table 2 for a summary).

Table 2: **Which backbone should I choose?** We list the top 3 most performant backbones (left to right) for various tasks and settings. Red corresponds to OOD evaluations and Green indicates overall comparisons.

Task	Good	Better	Best
1 Cls	ConvNeXt-B (IN-21k)	CLIP ViT-B (LAION-2B)	Sup. SwinV2-B (IN-21k,1k)
2 Det	Sup. ConvNeXt-B (IN-1k)	Sup. SwinV2-B (IN-21k,1k)	Sup. ConvNeXt-B (IN-21k)
3 Seg	Sup. ConvNeXt-B (IN-1k)	Sup. SwinV2-B (IN-21k,1k)	Sup. ConvNeXt-B (IN-21k)
4 Ret	CLIP ViT-B (LAION-2B)	Sup. SwinV2-B (IN-21k,1k)	Sup. ConvNeXt-B (IN-21k)
5 (OOD) Cls	CLIP ViT-B (LAION-2B)	Sup. SwinV2-B (IN-21k,1k)	Sup. ConvNeXt-B (IN-21k)
6 (OOD) Det	Sup. ConvNeXt-B (IN-21k)	Sup. ConvNeXt-T (IN-1k)	Sup. ConvNeXt-B (IN-1k)
7 All	CLIP ViT-B (LAION-2B)	Sup. SwinV2-B (IN-21k,1k)	Sup. ConvNeXt-B (IN-21k)

4.1 Task-Specific Backbones

Classification. For classification, across multiple datasets and experimental settings (fine-tuning, linear probing, full and low-shot training), we find "Supervised SwinV2-Base trained on IN-21k (finetuned on IN-1k)" to be the best performing backbone, followed by "CLIP ViT-Base" and "Supervised ConvNeXt-Base trained on IN-21k" (see row 1, Table 2).[2]

Object Detection & Segmentation. For object detection and instance segmentation, we find "Supervised ConvNeXt-Base trained on IN-21K" > "Supervised SwinV2-Base trained on IN-21k (finetuned on IN-1k)" > "Supervised ConvNeXt-Base trained on IN-1k".

Image Retrieval. For image retrieval, we find "Supervised ConvNeXt-Base trained on IN-21k" to be the best choice, with "Supervised SwinV2-Base trained on IN-21k (finetuned on IN-1k)" and "CLIP ViT-B trained on LAION-2B" being second and third.

(OOD) Classification. Across OOD evaluations for classification, we find "Supervised ConvNeXt-Base trained on IN-21k" > "Supervised SwinV2-B trained on IN-21k (finetuned on IN-1k)" > "CLIP ViT-Base trained on LAION-2B".

(OOD) Object Detection. For Syn→Real object detection, we find "Supervised ConvNeXt-Base trained on IN-1k" to be the best backbone, followed by "Supervised ConvNeXt-Tiny trained on IN-1k" and "Supervised ConvNeXt-Base trained on IN-21k".

4.2 Best Backbones Overall

For practitioners with no specific task in mind, the best performing models in terms of aggregate performance are "Supervised ConvNeXt-Base trained on IN-21k" followed by "Supervised SwinV2-Base trained on IN-21k (finetuned on IN-1k)" and "CLIP ViT-Base trained on LAION-2B". Overall, we note that backbones trained in a supervised fashion (SwinV2-Base, ConvNeXt-Base) or with vision and language supervision (CLIP ViT-Base) outperform the rest. Furthermore, we find that CLIP ViT-Base is closely followed by Supervised ViT-Base trained on IN-21k (finetuned on IN-1k). We more precisely compare approaches and analyze trends in Section 5.

4.3 Backbones on a Tight Budget

Many computer vision applications demand efficient backbones for fast or on-device inference. In this section, we benchmark three small backbones: RegNetX-400F [74], EfficientNet-B0 [84] and ResNet-18 [28] all pretrained in a supervised fashion on ImageNet-1k. We rank the performance of these small backbones on the set of tasks in Table 3. We find that EfficientNet-B0 performs best overall and across classification, retrieval, and OOD classification, followed by RegNetX-400MF and then ResNet-18. Interestingly, ResNets still outperform newer efficient architectures for detection and segmentation.

---

[2]To ensure fair comparisons across backbones, we exclude MiDaS variants evaluated on ImageNet for this comparison.

Table 3: **Which tiny backbone should I choose?** We rank the most performant very lightweight backbones (left to right) for various tasks and settings. Red correspond to OOD evaluations and Green indicates overall comparisons.

Task	Good	Better	Best
1 Cls	ResNet-18	RegNetX-400MF	EfficientNet-B0
2 Det	RegNetX-400MF	EfficientNet-B0	ResNet-18
3 Seg	RegNetX-400MF	EfficientNet-B0	ResNet-18
4 Ret	ResNet-18	RegNetX-400MF	EfficientNet-B0
5 (OOD) Cls	ResNet-18	RegNetX-400MF	EfficientNet-B0
6 (OOD) Det	EfficientNet-B0	ResNet-18	RegNetX-400MF
7 All	ResNet-18	RegNetX-400MF	EfficientNet-B0

5 Observations and Trends

▷ **A performance comparison of ViTs and CNNs. Modern architectures strongly outperform vanilla ViTs.** We see in Table 2 that the best performing backbone (ConvNeXt-Base) is convolutional, with a hierarchical transformer (SwinV2-Base) being a close second. The latter transformer architecture incorporates a strong spatial inductive bias. These findings suggest that the community should move past vanilla ViTs which are still used frequently. As a caveat, we do not evaluate very large models, and it is possible that ViTs might outperform their more advanced variants or convolutional networks at larger scales.

▷ **ViTs benefit more from scale than CNNs.** For the suite of backbones considered in BoB, we find that relative performance (z-scores) for both CNNs and ViTs correlates positively with parameter count but more so for ViTs (spearman $\rho = 0.58$) than for CNNs (spearman $\rho = 0.35$). Similarly, while overall relative performance correlates with the size of pretraining data, the correlation is again significantly higher for ViTs ($\rho = 0.72$) than for CNNs ($\rho = 0.33$). This observation indicates that benchmarking much larger backbones might yield different winners, possibly ones with transformer-based architectures.

▷ **Supervised or not? Supervised learning backbones dominate, but primarily because they are available pretrained on larger datasets. SSL backbones can outperform supervised pre-training with similar sized pre-training datasets.** We obtain the average score of the top 3 backbones within different pretraining styles, namely self-supervised, supervised with ImageNet-1K, and supervised with ImageNet-21K, for each task (see Appendix D). ConvNeXt and SwinV2 pretrained with supervision on ImageNet-21K outperform the SSL backbones on all tasks. The results suggest that we should try using advanced architectures, either convolutional or transformers, when applying SSL methods, and we should train on large datasets to compete with supervised learning. In these experiments, supervised pretraining checkpoints are often available trained on much larger datasets (ImageNet-21k). When comparing models pretrained on similarly sized datasets, SSL or vision-language pretraining methods achieve better performance on classification (both in- and out-of-distribution) and retrieval tasks, which heavily rely on the learned representations. However, supervised learning backbones maintain a decisive edge for detection and segmentation. We can also compare backbones which use the same ViT-Base architecture and find that SSL methods do outperform ImageNet-1k supervised backbones but are worse than ImageNet-21k trained backbones.

▷ **Performance across tasks is highly correlated.** Across tasks examined, we find a strong positive Spearman correlation between performance on task pairs (typically $\rho > 0.8$). This finding supports the current trend of general purpose foundation models for computer vision. Moreover, this finding also supports recent work which argues that a single inductive bias can solve a wide range of seemingly different problems [24]. However, it is noteworthy that the retrieval task exhibited a comparatively lower but still statistically significant correlation ($\rho = 0.49$) with respect to classification and retrieval ranking. This lower correlation can be attributed to the performance limitations of the MiDaS and MAE pretrained models in the context of retrieval. Upon removing these two backbones, the correlation coefficient ρ increased to 0.8, reinforcing the influence of the aforementioned models on the observed results.
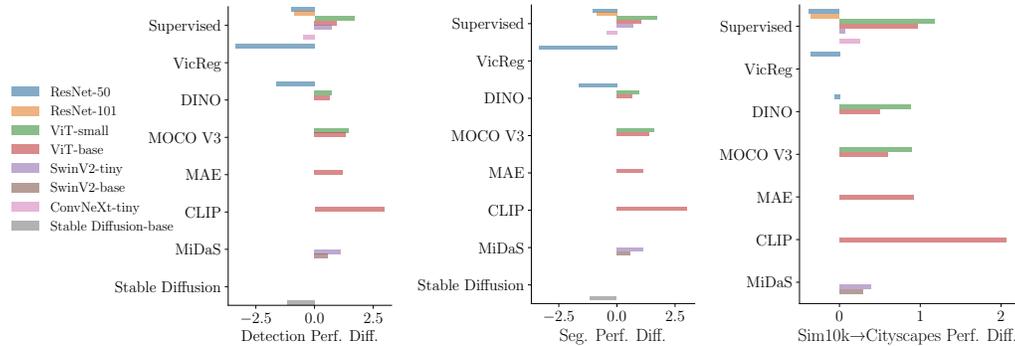
Figure 2: **Transformers benefit significantly more from end-to-end fine-tuning than CNNs on dense prediction tasks.** We visualize the difference in performance between end-to-end fine-tuning and only training the head atop a frozen feature extractor on different tasks. The x-axis is the difference in relative performance (fine-tuning z-score minus fixed backbone z-score). Across panels, the performance differences correlate between tasks.

▷ **Transformers excel under end-to-end fine-tuning while convolutional networks excel under linear probing.** For "linear probing" experiments, we freeze a pretrained backbone and only learn the head. Note that for detection and segmentation, the head is more than a linear layer. By inspecting the performance difference between the two fine-tuning strategies (Figure 2), we find that ViTs benefit significantly more from end-to-end fine-tuning compared to CNNs, both for supervised and self-supervised pretraining. See Figure 2 for a comparison on dense prediction tasks.

▷ **CLIP models and the promise of advanced architectures in vision-language modeling.** For almost all the tasks (except OOD detection), CLIP pretraining is the best among the vanilla vision transformers, even compared to ImageNet-21k supervised trained backbones. Among all the backbones, CLIP is only worse than ImageNet-21k trained SwinV2 and ConvNeXt, which shows the power of vision-language pretraining and again, suggests that we should consider more backbones other than plain ViTs when conducting self- or weakly-supervised learning.

▷ **What about generative backbones?** In contrast to models trained using supervised or self-supervised approaches with contrastive loss, backbones trained with a generative objective, such as MAE or Stable Diffusion, had comparatively inferior performance. We recommend caution when interpreting this result, as the evaluation of Stable Diffusion is currently limited to select tasks. Nonetheless, Stable Diffusion is a larger backbone than others considered in this benchmark and is trained on a very large dataset, yet it exhibits inferior performance.

▷ **Battle of the "small" backbones.** Keeping limited resources in mind, we also compare the "small" subset of backbones in BoB (< 30M parameters) – with ViT-Small, ConvNeXt-Tiny, Swin-Tiny and ResNet-50 architectures. Overall, we find Supervised ConvNeXt-T trained on IN-1k to be the best, followed by Supervised SwinV2-T trained on IN-1k and DINO ViT-S trained on IN-1k. Interestingly, supervised learning again dominates, and backbones pretrained on just IN-1k outperform ones trained on a considerably more diverse and larger dataset (MiDaS).

▷ **Performance vs. Speed?** Our analysis reveals a strong negative correlation ($\rho = -0.41$) between throughput (computed on NVIDIA RTX A5000) and average performance z-scores across all tasks when considering each backbone. This finding aligns with our previous observation that larger models tend to exhibit superior performance. Consequently, in order to achieve enhanced performance, one may need to sacrifice speed.

▷ **Monocular depth-estimation as a general purpose pretraining strategy.** In our experiments, MiDaS achieves performance competitive with that of top conventional supervised and SSL backbones at classification, object detection, and segmentation, even outside of the natural image domain, for example on satellite images. This observation suggests that depth-estimation may serve as a powerful and generalizable primary or auxiliary pretraining task for foundation models, supporting findings of Lao et al. [49].

▷ **Calibration and test likelihood are correlated with accuracy.** We measure expected calibration error (ECE) as well as test cross-entropy loss on the ImageNet test set. Whereas test likelihood is

strongly correlated with accuracy ($r = -0.8278$), ECE exhibits a weaker correlation ($r = -0.4876$). In both cases, we observe p-values under 0.05. We also note that self-supervised pretraining typically leads to inferior calibration.

▷ **CNNs and SSL are more adversarially robust.** We additionally measure the adversarial robustness of each backbone on the ImageNet test set using an ℓ_∞-constrained PGD attack with multiple radii (see Appendix Table 19). For each architecture where we possess self-supervised learning versions, we see that supervised pretraining always yields inferior robustness. Moreover, ViTs are more vulnerable to adversarial examples than convolutional networks. Notably, ConvNeXt is more adversarially robust even when trained in a supervised fashion.

6   Where Are Things Going From Here?

At the core of every computer vision model is a backbone. In our battle of the backbones, we compared more than 1,500 training runs to surface insights for computer vision practitioners and researchers. To guide practitioners, we analyzed the performance of publicly available vision backbones across a broad range of tasks from segmentation and detection to classification and retrieval. We found supervised ConvNext, supervised SwinV2, and CLIP models performed well across this broad range of tasks. For computationally constrained settings, in our battle of the "small" backbones we found smaller counterparts to the same archiectures supervised ConvNext-T and SwinV2, followed by DINO with a small ViT performed quite well. BoB offers practitioners a guide to select sensible backbones from the dizzying array of choices.

For researchers looking ahead, we also observed several notable trends. First, we found performance across tasks is strongly correlated, suggesting a shift away from specialized vision backbones to universal backbones that work well across a range of tasks. Next, we found throughput and performance are inverse related, suggesting scaling remains a promising avenue to improve backbones. Finally, we found that while our practical recommendations include many supervised models, in apple-to-apples comparisons to standard supervised training, self-supervised learning holds promise. By releasing all our experimental results along with code to put new backbones to the test, we hope BoB serves as a useful guide to both practitioners today and researchers looking ahead at tomorrow.

Limitations. We note that insights obtained from BoB are contingent on the vocabulary of tasks, backbones, and settings considered in this work. We intend for takeaways from this study to provide practical considerations useful for computer vision researchers, recognizing that such insights need to continuously evolve as more backbones are introduced and more tasks and settings are taken into account. Lastly, we note that studies in BoB focus mostly primarily on aspects related to performance, and exploration along other axes of importance (biases in models, etc.) remain.

Our benchmark does not include backbones larger than ConvNext-Base, aside from Stable Diffusion, and some rankings may change at a large scale. For instance, while we find that modern convolutional architectures pretrained via supervised learning perform best on most tasks, we also find that transformers benefit more from scale, both in terms of pretraining data and architecture size. It is possible that transformer backbones will pull ahead of convolutional backbones at very large scales.

7   Computation Cost and Carbon Footprint

The experiments in this paper took a cumulative 127k GPU hours on `NVIDIA RTX A100` cards. Assuming the GPUs were running with an average carbon efficiency of 0.37 kgCO$_2$eq/kWh, the total emissions are estimated to be 11792.36 kgCO$_2$eq [48].

Acknowledgements

References

[1] Hangbo Bao, Li Dong, Songhao Piao, and Furu Wei. Beit: Bert pre-training of image transformers. *arXiv preprint arXiv:2106.08254*, 2021.

[2] Andrei Barbu, David Mayo, Julian Alverio, William Luo, Christopher Wang, Dan Gutfreund, Josh Tenenbaum, and Boris Katz. Objectnet: A large-scale bias-controlled dataset for pushing the limits of object recognition models. *Advances in neural information processing systems*, 32, 2019.

[3] Adrien Bardes, Jean Ponce, and Yann LeCun. Vicreg: Variance-invariance-covariance regularization for self-supervised learning. In *International Conference on Learning Representations*, 2022.

[4] Adrien Bardes, Jean Ponce, and Yann LeCun. Vicregl: Self-supervised learning of local visual features. In *Advances in Neural Information Processing Systems*, 2022.

[5] Zhaowei Cai and Nuno Vasconcelos. Cascade r-cnn: Delving into high quality object detection. In *Proceedings of the IEEE conference on computer vision and pattern recognition*, pages 6154–6162, 2018.

[6] Zhaowei Cai, Avinash Ravichandran, Paolo Favaro, Manchen Wang, Davide Modolo, Rahul Bhotika, Zhuowen Tu, and Stefano Soatto. Semi-supervised vision transformers at scale. *arXiv preprint arXiv:2208.05688*, 2022.

[7] Nicolas Carion, Francisco Massa, Gabriel Synnaeve, Nicolas Usunier, Alexander Kirillov, and Sergey Zagoruyko. End-to-end object detection with transformers. In *Computer Vision–ECCV 2020: 16th European Conference, Glasgow, UK, August 23–28, 2020, Proceedings, Part I 16*, pages 213–229. Springer, 2020.

[8] Mathilde Caron, Hugo Touvron, Ishan Misra, Hervé Jégou, Julien Mairal, Piotr Bojanowski, and Armand Joulin. Emerging properties in self-supervised vision transformers. In *Proceedings of the IEEE/CVF international conference on computer vision*, pages 9650–9660, 2021.

[9] Kai Chen, Jiaqi Wang, Jiangmiao Pang, Yuhang Cao, Yu Xiong, Xiaoxiao Li, Shuyang Sun, Wansen Feng, Ziwei Liu, Jiarui Xu, et al. Mmdetection: Open mmlab detection toolbox and benchmark. *arXiv preprint arXiv:1906.07155*, 2019.

[10] Ting Chen, Simon Kornblith, Mohammad Norouzi, and Geoffrey Hinton. A simple framework for contrastive learning of visual representations. In *International conference on machine learning*, pages 1597–1607. PMLR, 2020.

[11] Wei Chen, Yu Liu, Weiping Wang, Erwin Bakker, Theodoros Georgiou, Paul Fieguth, Li Liu, and Michael S Lew. Deep learning for instance retrieval: A survey. *arXiv preprint arXiv:2101.11282*, 2021.

[12] Xinlei Chen, Saining Xie, and Kaiming He. An empirical study of training self-supervised vision transformers. In *Proceedings of the IEEE/CVF International Conference on Computer Vision*, pages 9640–9649, 2021.

[13] Yuhua Chen, Wen Li, Christos Sakaridis, Dengxin Dai, and Luc Van Gool. Domain adaptive faster r-cnn for object detection in the wild. In *Proceedings of the IEEE conference on computer vision and pattern recognition*, pages 3339–3348, 2018.

[14] Zhe Chen, Yuchen Duan, Wenhai Wang, Junjun He, Tong Lu, Jifeng Dai, and Yu Qiao. Vision transformer adapter for dense predictions. In *The Eleventh International Conference on Learning Representations*, 2023.

[15] Marius Cordts, Mohamed Omran, Sebastian Ramos, Timo Rehfeld, Markus Enzweiler, Rodrigo Benenson, Uwe Franke, Stefan Roth, and Bernt Schiele. The cityscapes dataset for semantic urban scene understanding. In *Proceedings of the IEEE conference on computer vision and pattern recognition*, pages 3213–3223, 2016.

[16] Ekin D Cubuk, Barret Zoph, Jonathon Shlens, and Quoc V Le. Randaugment: Practical automated data augmentation with a reduced search space. In *Proceedings of the IEEE/CVF conference on computer vision and pattern recognition workshops*, pages 702–703, 2020.

[17] Jia Deng, Wei Dong, Richard Socher, Li-Jia Li, Kai Li, and Li Fei-Fei. Imagenet: A large-scale hierarchical image database. In *2009 IEEE conference on computer vision and pattern recognition*, pages 248–255. Ieee, 2009.

[18] Alexey Dosovitskiy, Lucas Beyer, Alexander Kolesnikov, Dirk Weissenborn, Xiaohua Zhai, Thomas Unterthiner, Mostafa Dehghani, Matthias Minderer, Georg Heigold, Sylvain Gelly, et al. An image is worth 16x16 words: Transformers for image recognition at scale. *arXiv preprint arXiv:2010.11929*, 2020.

[19] Matthijs Douze, Hervé Jégou, Harsimrat Sandhawalia, Laurent Amsaleg, and Cordelia Schmid. Evaluation of gist descriptors for web-scale image search. In *Proceedings of the ACM International Conference on Image and Video Retrieval*, pages 1–8, 2009.

[20] Shiv Ram Dubey. A decade survey of content based image retrieval using deep learning. *IEEE Transactions on Circuits and Systems for Video Technology*, 32(5):2687–2704, 2021.

[21] Linus Ericsson, Henry Gouk, and Timothy M Hospedales. How well do self-supervised models transfer? In *Proceedings of the IEEE/CVF Conference on Computer Vision and Pattern Recognition*, pages 5414–5423, 2021.

[22] Amin Ghiasi, Hamid Kazemi, Eitan Borgnia, Steven Reich, Manli Shu, Micah Goldblum, Andrew Gordon Wilson, and Tom Goldstein. What do vision transformers learn? a visual exploration. *arXiv preprint arXiv:2212.06727*, 2022.

[23] Ross Girshick, Jeff Donahue, Trevor Darrell, and Jitendra Malik. Rich feature hierarchies for accurate object detection and semantic segmentation. In *Proceedings of the IEEE conference on computer vision and pattern recognition*, pages 580–587, 2014.

[24] Micah Goldblum, Marc Finzi, Keefer Rowan, and Andrew Gordon Wilson. The no free lunch theorem, kolmogorov complexity, and the role of inductive biases in machine learning. *arXiv preprint arXiv:2304.05366*, 2023.

[25] Priya Goyal, Dhruv Mahajan, Abhinav Gupta, and Ishan Misra. Scaling and benchmarking self-supervised visual representation learning. In *Proceedings of the ieee/cvf International Conference on computer vision*, pages 6391–6400, 2019.

[26] Priya Goyal, Benjamin Lefaudeux, Mannat Singh, Jeremy Reizenstein, Vinicius Reis, Min Xu, , Matthew Leavitt, Mathilde Caron, Piotr Bojanowski, Armand Joulin, and Ishan Misra. Vissl. https://github.com/facebookresearch/vissl, 2021.

[27] Agrim Gupta, Piotr Dollar, and Ross Girshick. Lvis: A dataset for large vocabulary instance segmentation. In *Proceedings of the IEEE/CVF conference on computer vision and pattern recognition*, pages 5356–5364, 2019.

[28] Kaiming He, Xiangyu Zhang, Shaoqing Ren, and Jian Sun. Deep residual learning for image recognition. In *Proceedings of the IEEE conference on computer vision and pattern recognition*, pages 770–778, 2016.

[29] Kaiming He, Ross Girshick, and Piotr Dollár. Rethinking imagenet pre-training. In *Proceedings of the IEEE/CVF International Conference on Computer Vision*, pages 4918–4927, 2019.

[30] Kaiming He, Xinlei Chen, Saining Xie, Yanghao Li, Piotr Dollár, and Ross Girshick. Masked autoencoders are scalable vision learners. In *Proceedings of the IEEE/CVF Conference on Computer Vision and Pattern Recognition*, pages 16000–16009, 2022.

[31] Patrick Helber, Benjamin Bischke, Andreas Dengel, and Damian Borth. Eurosat: A novel dataset and deep learning benchmark for land use and land cover classification. *IEEE Journal of Selected Topics in Applied Earth Observations and Remote Sensing*, 12(7):2217–2226, 2019.

[32] Dan Hendrycks and Thomas Dietterich. Benchmarking neural network robustness to common corruptions and perturbations. *arXiv preprint arXiv:1903.12261*, 2019.

[33] Dan Hendrycks, Steven Basart, Norman Mu, Saurav Kadavath, Frank Wang, Evan Dorundo, Rahul Desai, Tyler Zhu, Samyak Parajuli, Mike Guo, et al. The many faces of robustness: A critical analysis of out-of-distribution generalization. In *Proceedings of the IEEE/CVF International Conference on Computer Vision*, pages 8340–8349, 2021.

[34] Dan Hendrycks, Kevin Zhao, Steven Basart, Jacob Steinhardt, and Dawn Song. Natural adversarial examples. In *Proceedings of the IEEE/CVF Conference on Computer Vision and Pattern Recognition*, pages 15262–15271, 2021.

[35] Xinyu Huang, Xinjing Cheng, Qichuan Geng, Binbin Cao, Dingfu Zhou, Peng Wang, Yuanqing Lin, and Ruigang Yang. The apolloscape dataset for autonomous driving. In *Proceedings of the IEEE conference on computer vision and pattern recognition workshops*, pages 954–960, 2018.

[36] Sergey Ioffe and Christian Szegedy. Batch normalization: Accelerating deep network training by reducing internal covariate shift. In *International conference on machine learning*, pages 448–456. pmlr, 2015.

[37] Jeremy Irvin, Pranav Rajpurkar, Michael Ko, Yifan Yu, Silviana Ciurea-Ilcus, Chris Chute, Henrik Marklund, Behzad Haghgoo, Robyn Ball, Katie Shpanskaya, et al. Chexpert: A large chest radiograph dataset with uncertainty labels and expert comparison. In *Proceedings of the AAAI conference on artificial intelligence*, volume 33, pages 590–597, 2019.

[38] Matthew Johnson-Roberson, Charles Barto, Rounak Mehta, Sharath Nittur Sridhar, Karl Rosaen, and Ram Vasudevan. Driving in the matrix: Can virtual worlds replace human-generated annotations for real world tasks? In *2017 IEEE International Conference on Robotics and Automation (ICRA)*, pages 746–753. IEEE, 2017.

[39] Rajiv Kapoor, Deepak Sharma, and Tarun Gulati. State of the art content based image retrieval techniques using deep learning: a survey. *Multimedia Tools and Applications*, 80(19):29561–29583, 2021.

[40] Jacob Devlin Ming-Wei Chang Kenton and Lee Kristina Toutanova. Bert: Pre-training of deep bidirectional transformers for language understanding. In *Proceedings of NAACL-HLT*, pages 4171–4186, 2019.

[41] Donghyun Kim, Kaihong Wang, Stan Sclaroff, and Kate Saenko. A broad study of pre-training for domain generalization and adaptation. In *Computer Vision–ECCV 2022: 17th European Conference, Tel Aviv, Israel, October 23–27, 2022, Proceedings, Part XXXIII*, pages 621–638. Springer, 2022.

[42] Youngjung Kim, Hyungjoo Jung, Dongbo Min, and Kwanghoon Sohn. Deep monocular depth estimation via integration of global and local predictions. *IEEE transactions on Image Processing*, 27(8):4131–4144, 2018.

[43] Pang Wei Koh, Shiori Sagawa, Henrik Marklund, Sang Michael Xie, Marvin Zhang, Akshay Balsubramani, Weihua Hu, Michihiro Yasunaga, Richard Lanas Phillips, Irena Gao, et al. Wilds: A benchmark of in-the-wild distribution shifts. In *International Conference on Machine Learning*, pages 5637–5664. PMLR, 2021.

[44] Alexander Kolesnikov, Xiaohua Zhai, and Lucas Beyer. Revisiting self-supervised visual representation learning. In *Proceedings of the IEEE/CVF conference on computer vision and pattern recognition*, pages 1920–1929, 2019.

[45] Simon Kornblith, Jonathon Shlens, and Quoc V Le. Do better imagenet models transfer better? In *Proceedings of the IEEE/CVF conference on computer vision and pattern recognition*, pages 2661–2671, 2019.

[46] Alex Krizhevsky, Geoffrey Hinton, et al. Learning multiple layers of features from tiny images. 2009.

[47] Alex Krizhevsky, Ilya Sutskever, and Geoffrey E Hinton. Imagenet classification with deep convolutional neural networks. *Communications of the ACM*, 60(6):84–90, 2017.

[48] Alexandre Lacoste, Alexandra Luccioni, Victor Schmidt, and Thomas Dandres. Quantifying the carbon emissions of machine learning. *arXiv preprint arXiv:1910.09700*, 2019.

[49] Dong Lao, Alex Wong, and Stefano Soatto. Depth estimation vs classification as pre-training for semantic segmentation. *arXiv preprint arXiv:2203.13987*, 2022.

[50] Da Li, Yongxin Yang, Yi-Zhe Song, and Timothy M Hospedales. Deeper, broader and artier domain generalization. In *Proceedings of the IEEE international conference on computer vision*, pages 5542–5550, 2017.

[51] Yanghao Li, Saining Xie, Xinlei Chen, Piotr Dollar, Kaiming He, and Ross Girshick. Benchmarking detection transfer learning with vision transformers. *arXiv preprint arXiv:2111.11429*, 2021.

[52] Yanghao Li, Hanzi Mao, Ross Girshick, and Kaiming He. Exploring plain vision transformer backbones for object detection. In *Computer Vision–ECCV 2022: 17th European Conference, Tel Aviv, Israel, October 23–27, 2022, Proceedings, Part IX*, pages 280–296. Springer, 2022.

[53] Zhengqi Li and Noah Snavely. Megadepth: Learning single-view depth prediction from internet photos. In *Proceedings of the IEEE conference on computer vision and pattern recognition*, pages 2041–2050, 2018.

[54] Tsung-Yi Lin, Michael Maire, Serge Belongie, James Hays, Pietro Perona, Deva Ramanan, Piotr Dollár, and C Lawrence Zitnick. Microsoft coco: Common objects in context. In *Computer Vision–ECCV 2014: 13th European Conference, Zurich, Switzerland, September 6-12, 2014, Proceedings, Part V 13*, pages 740–755. Springer, 2014.

[55] Tsung-Yi Lin Lin, Michael Maire, Serge Belongie, James Hays, Pietro Perona, Deva Ramanan, Piotr Dollar, and C Lawrence Zitnick. Coco detection evaluation. http://cocodataset.org/#detection-eval, 2018.

[56] Ze Liu, Yutong Lin, Yue Cao, Han Hu, Yixuan Wei, Zheng Zhang, Stephen Lin, and Baining Guo. Swin transformer: Hierarchical vision transformer using shifted windows. In *Proceedings of the IEEE/CVF international conference on computer vision*, pages 10012–10022, 2021.

[57] Ze Liu, Han Hu, Yutong Lin, Zhuliang Yao, Zhenda Xie, Yixuan Wei, Jia Ning, Yue Cao, Zheng Zhang, Li Dong, et al. Swin transformer v2: Scaling up capacity and resolution. In *Proceedings of the IEEE/CVF conference on computer vision and pattern recognition*, pages 12009–12019, 2022.

[58] Zhuang Liu, Hanzi Mao, Chao-Yuan Wu, Christoph Feichtenhofer, Trevor Darrell, and Saining Xie. A convnet for the 2020s. In *Proceedings of the IEEE/CVF Conference on Computer Vision and Pattern Recognition*, pages 11976–11986, 2022.

[59] Jonathan Long, Evan Shelhamer, and Trevor Darrell. Fully convolutional networks for semantic segmentation. In *Proceedings of the IEEE conference on computer vision and pattern recognition*, pages 3431–3440, 2015.

[60] Ilya Loshchilov and Frank Hutter. Decoupled weight decay regularization. *arXiv preprint arXiv:1711.05101*, 2017.

[61] Subhransu Maji, Esa Rahtu, Juho Kannala, Matthew Blaschko, and Andrea Vedaldi. Fine-grained visual classification of aircraft. *arXiv preprint arXiv:1306.5151*, 2013.

[62] Moritz Menze and Andreas Geiger. Object scene flow for autonomous vehicles. In *Proceedings of the IEEE conference on computer vision and pattern recognition*, pages 3061–3070, 2015.

[63] Mazda Moayeri, Sahil Singla, and Soheil Feizi. Hard imagenet: Segmentations for objects with strong spurious cues. In *Thirty-sixth Conference on Neural Information Processing Systems Datasets and Benchmarks Track*, 2022.

[64] Gerhard Neuhold, Tobias Ollmann, Samuel Rota Bulo, and Peter Kontschieder. The mapillary vistas dataset for semantic understanding of street scenes. In *Proceedings of the IEEE international conference on computer vision*, pages 4990–4999, 2017.

[65] Maria-Elena Nilsback and Andrew Zisserman. Automated flower classification over a large number of classes. In *2008 Sixth Indian Conference on Computer Vision, Graphics & Image Processing*, pages 722–729. IEEE, 2008.

[66] Xingchao Peng, Ben Usman, Neela Kaushik, Judy Hoffman, Dequan Wang, and Kate Saenko. Visda: The visual domain adaptation challenge. *arXiv preprint arXiv:1710.06924*, 2017.

[67] Xingchao Peng, Qinxun Bai, Xide Xia, Zijun Huang, Kate Saenko, and Bo Wang. Moment matching for multi-source domain adaptation. In *Proceedings of the IEEE/CVF international conference on computer vision*, pages 1406–1415, 2019.

[68] Florent Perronnin, Yan Liu, and Jean-Michel Renders. A family of contextual measures of similarity between distributions with application to image retrieval. In *2009 IEEE Conference on computer vision and pattern recognition*, pages 2358–2365. IEEE, 2009.

[69] James Philbin, Ondrej Chum, Michael Isard, Josef Sivic, and Andrew Zisserman. Object retrieval with large vocabularies and fast spatial matching. In *2007 IEEE conference on computer vision and pattern recognition*, pages 1–8. IEEE, 2007.

[70] James Philbin, Ondrej Chum, Michael Isard, Josef Sivic, and Andrew Zisserman. Lost in quantization: Improving particular object retrieval in large scale image databases. In *2008 IEEE conference on computer vision and pattern recognition*, pages 1–8. IEEE, 2008.

[71] Joaquin Quinonero-Candela, Masashi Sugiyama, Anton Schwaighofer, and Neil D Lawrence. *Dataset shift in machine learning*. Mit Press, 2008.

[72] Filip Radenović, Ahmet Iscen, Giorgos Tolias, Yannis Avrithis, and Ondřej Chum. Revisiting oxford and paris: Large-scale image retrieval benchmarking. In *Proceedings of the IEEE conference on computer vision and pattern recognition*, pages 5706–5715, 2018.

[73] Alec Radford, Jong Wook Kim, Chris Hallacy, Aditya Ramesh, Gabriel Goh, Sandhini Agarwal, Girish Sastry, Amanda Askell, Pamela Mishkin, Jack Clark, et al. Learning transferable visual models from natural language supervision. In *International conference on machine learning*, pages 8748–8763. PMLR, 2021.

[74] Ilija Radosavovic, Raj Prateek Kosaraju, Ross Girshick, Kaiming He, and Piotr Dollár. Designing network design spaces. In *Proceedings of the IEEE/CVF conference on computer vision and pattern recognition*, pages 10428–10436, 2020.

[75] René Ranftl, Katrin Lasinger, David Hafner, Konrad Schindler, and Vladlen Koltun. Towards robust monocular depth estimation: Mixing datasets for zero-shot cross-dataset transfer. *IEEE transactions on pattern analysis and machine intelligence*, 44(3):1623–1637, 2020.

[76] Benjamin Recht, Rebecca Roelofs, Ludwig Schmidt, and Vaishaal Shankar. Do imagenet classifiers generalize to imagenet? In *International conference on machine learning*, pages 5389–5400. PMLR, 2019.

[77] Robin Rombach, Andreas Blattmann, Dominik Lorenz, Patrick Esser, and Björn Ommer. High-resolution image synthesis with latent diffusion models. In *Proceedings of the IEEE/CVF Conference on Computer Vision and Pattern Recognition*, pages 10684–10695, 2022.

[78] Yangjun Ruan, Yann Dubois, and Chris J Maddison. Optimal representations for covariate shift. *arXiv preprint arXiv:2201.00057*, 2021.

[79] Olga Russakovsky, Jia Deng, Hao Su, Jonathan Krause, Sanjeev Satheesh, Sean Ma, Zhiheng Huang, Andrej Karpathy, Aditya Khosla, Michael Bernstein, et al. Imagenet large scale visual recognition challenge. *International journal of computer vision*, 115:211–252, 2015.

[80] Christos Sakaridis, Dengxin Dai, and Luc Van Gool. Semantic foggy scene understanding with synthetic data. *International Journal of Computer Vision*, 126:973–992, 2018.

[81] Christoph Schuhmann, Romain Beaumont, Richard Vencu, Cade W Gordon, Ross Wightman, Mehdi Cherti, Theo Coombes, Aarush Katta, Clayton Mullis, Mitchell Wortsman, et al. Laion-5b: An open large-scale dataset for training next generation image-text models. In *Thirty-sixth Conference on Neural Information Processing Systems Datasets and Benchmarks Track*, 2022.

[82] Nathan Silberman, Derek Hoiem, Pushmeet Kohli, and Rob Fergus. Indoor segmentation and support inference from rgbd images. *ECCV (5)*, 7576:746–760, 2012.

[83] Peize Sun, Rufeng Zhang, Yi Jiang, Tao Kong, Chenfeng Xu, Wei Zhan, Masayoshi Tomizuka, Lei Li, Zehuan Yuan, Changhu Wang, et al. Sparse r-cnn: End-to-end object detection with learnable proposals. In *Proceedings of the IEEE/CVF conference on computer vision and pattern recognition*, pages 14454–14463, 2021.

[84] Mingxing Tan and Quoc Le. Efficientnet: Rethinking model scaling for convolutional neural networks. In *International conference on machine learning*, pages 6105–6114. PMLR, 2019.

[85] Hugo Touvron, Matthieu Cord, Matthijs Douze, Francisco Massa, Alexandre Sablayrolles, and Hervé Jégou. Training data-efficient image transformers & distillation through attention. In *International conference on machine learning*, pages 10347–10357. PMLR, 2021.

[86] Tuan Truong, Sadegh Mohammadi, and Matthias Lenga. How transferable are self-supervised features in medical image classification tasks? In *Machine Learning for Health*, pages 54–74. PMLR, 2021.

[87] Eric Tzeng, Judy Hoffman, Kate Saenko, and Trevor Darrell. Adversarial discriminative domain adaptation. In *Proceedings of the IEEE conference on computer vision and pattern recognition*, pages 7167–7176, 2017.

[88] Grant Van Horn, Oisin Mac Aodha, Yang Song, Yin Cui, Chen Sun, Alex Shepard, Hartwig Adam, Pietro Perona, and Serge Belongie. The inaturalist species classification and detection dataset. In *Proceedings of the IEEE conference on computer vision and pattern recognition*, pages 8769–8778, 2018.

[89] Ashish Vaswani, Noam Shazeer, Niki Parmar, Jakob Uszkoreit, Llion Jones, Aidan N Gomez, Łukasz Kaiser, and Illia Polosukhin. Attention is all you need. *Advances in neural information processing systems*, 30, 2017.

[90] Hemanth Venkateswara, Jose Eusebio, Shayok Chakraborty, and Sethuraman Panchanathan. Deep hashing network for unsupervised domain adaptation. In *Proceedings of the IEEE conference on computer vision and pattern recognition*, pages 5018–5027, 2017.

[91] Catherine Wah, Steve Branson, Peter Welinder, Pietro Perona, and Serge Belongie. The caltech-ucsd birds-200-2011 dataset. 2011.

[92] Chaoyang Wang, Simon Lucey, Federico Perazzi, and Oliver Wang. Web stereo video supervision for depth prediction from dynamic scenes. In *2019 International Conference on 3D Vision (3DV)*, pages 348–357. IEEE, 2019.

[93] Haohan Wang, Songwei Ge, Zachary Lipton, and Eric P Xing. Learning robust global representations by penalizing local predictive power. In *Advances in Neural Information Processing Systems*, pages 10506–10518, 2019.

[94] Qiang Wang, Shizhen Zheng, Qingsong Yan, Fei Deng, Kaiyong Zhao, and Xiaowen Chu. Irs: A large naturalistic indoor robotics stereo dataset to train deep models for disparity and surface normal estimation. *arXiv preprint arXiv:1912.09678*, 2019.

[95] Shuang Wang and Shuqiang Jiang. Instre: a new benchmark for instance-level object retrieval and recognition. *ACM Transactions on Multimedia Computing, Communications, and Applications (TOMM)*, 11(3):1–21, 2015.

[96] Wenshan Wang, Delong Zhu, Xiangwei Wang, Yaoyu Hu, Yuheng Qiu, Chen Wang, Yafei Hu, Ashish Kapoor, and Sebastian Scherer. Tartanair: A dataset to push the limits of visual slam. In *2020 IEEE/RSJ International Conference on Intelligent Robots and Systems (IROS)*, pages 4909–4916. IEEE, 2020.

[97] Ryan Webster, Julien Rabin, Loic Simon, and Frederic Jurie. On the de-duplication of laion-2b. *arXiv preprint arXiv:2303.12733*, 2023.

[98] T. Weyand, A. Araujo, B. Cao, and J. Sim. Google Landmarks Dataset v2 - A Large-Scale Benchmark for Instance-Level Recognition and Retrieval. In *Proc. CVPR*, 2020.

[99] Tobias Weyand, Andre Araujo, Bingyi Cao, and Jack Sim. Google landmarks dataset v2-a large-scale benchmark for instance-level recognition and retrieval. In *Proceedings of the IEEE/CVF conference on computer vision and pattern recognition*, pages 2575–2584, 2020.

[100] Ross Wightman, Hugo Touvron, and Hervé Jégou. Resnet strikes back: An improved training procedure in timm. *arXiv preprint arXiv:2110.00476*, 2021.

[101] Ke Xian, Chunhua Shen, Zhiguo Cao, Hao Lu, Yang Xiao, Ruibo Li, and Zhenbo Luo. Monocular relative depth perception with web stereo data supervision. In *Proceedings of the IEEE Conference on Computer Vision and Pattern Recognition*, pages 311–320, 2018.

[102] Ke Xian, Jianming Zhang, Oliver Wang, Long Mai, Zhe Lin, and Zhiguo Cao. Structure-guided ranking loss for single image depth prediction. In *Proceedings of the IEEE/CVF Conference on Computer Vision and Pattern Recognition*, pages 611–620, 2020.

[103] Junfei Xiao, Yutong Bai, Alan Yuille, and Zongwei Zhou. Delving into masked autoencoders for multi-label thorax disease classification. In *Proceedings of the IEEE/CVF Winter Conference on Applications of Computer Vision*, pages 3588–3600, 2023.

[104] Yao Yao, Zixin Luo, Shiwei Li, Jingyang Zhang, Yufan Ren, Lei Zhou, Tian Fang, and Long Quan. Blendedmvs: A large-scale dataset for generalized multi-view stereo networks. In *Proceedings of the IEEE/CVF Conference on Computer Vision and Pattern Recognition*, pages 1790–1799, 2020.

[105] Fisher Yu, Haofeng Chen, Xin Wang, Wenqi Xian, Yingying Chen, Fangchen Liu, Vashisht Madhavan, and Trevor Darrell. Bdd100k: A diverse driving dataset for heterogeneous multitask learning. In *Proceedings of the IEEE/CVF conference on computer vision and pattern recognition*, pages 2636–2645, 2020.

[106] Jiahui Yu, Zirui Wang, Vijay Vasudevan, Legg Yeung, Mojtaba Seyedhosseini, and Yonghui Wu. Coca: Contrastive captioners are image-text foundation models. *arXiv preprint arXiv:2205.01917*, 2022.

[107] Xiaohua Zhai, Joan Puigcerver, Alexander Kolesnikov, Pierre Ruyssen, Carlos Riquelme, Mario Lucic, Josip Djolonga, Andre Susano Pinto, Maxim Neumann, Alexey Dosovitskiy, et al. A large-scale study of representation learning with the visual task adaptation benchmark. *arXiv preprint arXiv:1910.04867*, 2019.

[108] Wengang Zhou, Houqiang Li, and Qi Tian. Recent advance in content-based image retrieval: A literature survey. *arXiv preprint arXiv:1706.06064*, 2017.

A Additional Related Work

Classification benchmarks. Image classification is the most common task in computer vision, and we have multiple benchmarks. For example, the `timm` library [100] benchmarks ImageNet classification performance across loads of backbones trained with different methods and on different datasets. In addition, we have dataset-specific benchmarks, such as "paperwithcode"[3]. The latter contains multiple datasets and methods, but it lacks systematic analysis among these results. Almost all the self-supervised learning method papers perform their own evaluation for image classification. To accelerate the research cycle in self-supervised learning, VISSL [26] provides a library for implementing SSL methods and evaluations. In this work, we evaluate various backbones trained in both self-supervised and supervised fashion, and on multiple datasets on different domains (natural images, satellite maps, and medical images). Moreover, we benchmark these backbones and datasets with exactly the same learning setting and conduct a thorough analysis of the collected results, which we believe is essential and helpful to practitioners.

Object detection and segmentation benchmarks. Benchmarking backbones for object detection and segmentation has been an active area of research. Several works have focused on evaluating and comparing the performance of various backbone architectures for these tasks [51, 52, 29, 9]. Popular backbone networks such as supervised pretrained ResNet have been extensively utilized and compared, while modern feature extractors such as vision-language models and self-supervised learning models have not been extensively studied. These studies either focus on a limited subset of backbones or incorporate diverse detectors with varying backbones, thereby hindering an accurate comparison. To the best of our knowledge, we are the first to present a comprehensive study of the various backbones with various architectures and pretraining methods for object detection and instance segmentation.

Out-of-distribution generalization benchmarks. Several prior works have benchmarked the out-of-distribution performance of visual models. For image classification, these have included variants of ImageNet [32–34, 93, 76, 63], synthetic-to-real adaptation benchmarks [66], and benchmarks with images belonging to varied domains including paintings, clipart, etc. [50, 67, 90, 87], sometimes even spanning multiple modalities and applications [43]. Similarly for object detection, several OOD generalization benchmarks have been fashioned from sim-to-real, cross-weather, and cross-city self-driving datasets [38, 15, 105, 80, 64]. Recently, [41] conducted a broad study of pretraining strategies for domain adaptation and generalization. In this work, we perform a similar study but on a larger scale and also include a diverse suite of backbones designed for varied tasks.

Image retrieval benchmarks. To the best of our knowledge, our study represents the first comprehensive examination of multiple pretrained deep learning backbones for image retrieval task. While previous survey papers [11, 108, 20, 39] have explanations of various types of deep learning methods, such as off-the-shelf models trained in an unsupervised or supervised fashion, single pass, and multiple pass methods, none have **quantitatively** analyzed these backbones. Therefore, our work fills this crucial gap in the existing literature.

B An Extended Guide to BoB

B.1 The Architectures

Below is a list of all architectures we compare. As different neural network architectures are believed to have distinct properties, from invariances to a reliance on different Fourier frequencies, evaluating a variety of architectures will allow us examine potential benefits of architectural differences. Many of the pretraining strategies we evaluate are accompanied by multiple checkpoints with different architectures or sizes, so we include multiple versions of each. We describe architectural modifications to these backbones for object detection and segmentation in Section 3.2.

- **ResNet [28]:** These are the staple convolutional neural networks we all know and love, complete with skip connections and batch normalization [36]. We include experiments on ResNet-50 and ResNet-101 backbones.

---

[3]https://paperswithcode.com/

- **ConvNeXt [58]:** ConvNeXt is a purely convolutional network with numerous modern architectural improvements including depthwise convolutions, inverted bottleneck blocks, large convolutional kernels, and a larger proportion of layers allocated to the third stage. This architecture improves performance of convolutional architectures at scale while maintaining their strong object detection and segmentation capabilities. We include experiments on ConvNeXt-Tiny and ConvNeXt-Base.

- **Vision Transformer [18]:** Vision transformers (ViTs) were derived from transformer language models [89] and inherit their multi-headed self-attention (MHSA) and position-wise feed-forward network (FFN) components. Unlike ResNets, ViTs do not encode translation equivariance, and they only encode locality by embedding images on a patch-by-patch basis. We include experiments on ViT-Small and ViT-Base.

- **Swin Transformer V2 [57]:** Swin Transformer [56] is a transformer architecture which incorporates hierarchical representations, translation invariance, and increased locality and efficiency into ViTs by only performing attention within spatial windows and merging these windows iteratively. SwinV2 is equipped with several modifications which improve scalability and transferability across input resolutions. We include experiments on SwinV2-Tiny and SwinV2-Base. For SwinV2-Base, unless otherwise stated, we use the model with a window size of 24.

- **Stable Diffusion encoder [77]:** Stable Diffusion is a text-to-image generative diffusion model which conducts diffusion in a latent space. We include experiments with a backbone formed by the learned encoder that converts images from pixel-space into the latent space where diffusion is performed followed by Stable Diffusion's U-Net, and we freeze the text encoder, using its frozen embedding. The encoder uses a convolutional architecture with added attention mechanisms. More details can be found in Rombach et al. [77].

B.2 The Pretraining Algorithms

The primary source of diversity amongst the backbones we consider stems from their different pretraining algorithms. We choose prototypical examples of categories including supervised learning, self-supervised learning (SSL), and vision-language since such types of pretraining routines are widely believed to confer their own unique properties. For instance, SSL backbones are thought to extract more transferable features [86], while vision-language models are thought to resist domain shifts [78].

- **Classification:** We include image classifiers pretrained on ImageNet-1k and -21k [17]. ImageNet pretraining has long been the de facto choice for computer vision systems.

- **MiDaS [75]:** MiDaS is trained in a supervised fashion for monocular depth estimation. In this task, the model accepts a natural image and outputs a dense 2D array of depth values representing the distance of the scene from the image plane.

- **MoCo v3 [12]:** Contrastive learning is a popular approach to SSL in computer vision which encourages a model extract similar features corresponding to different augmentations of the same image, called *positive pairs* and dissimilar features corresponding to different images, called *negative pairs*. MoCo v3 is a high-performing variant which employs a momentum encoder and multi-crop training as well as prediction and projection heads.

- **VICReg [3]:** Instead of adopting contrastive learning and negative pairs, VICReg avoids feature vectors collapsing towards a constant during SSL by regularizing their variance and covariance. VICRegL is a version which also applies the VICReg criterion to local features to teach the model to extract localization information in its features for downstream dense prediction tasks [4].

- **DINO [8]:** Much like MoCo v3, DINO uses a momentum encoder and multi-crop SSL, but DINO swaps out contrastive learning for self-distillation, demonstrating strong performance on ViTs with a small patch size.

- **MAE [30]:** Masked Autoencoders (MAE) use a distinct style of SSL adapted from masked language modeling [40]. MAE models are trained to reconstruct masked out input patches, unlike the above 3 models which instead match the features of augmented images.

- **CLIP [73]:** CLIP also uses contrastive learning, but on image-caption pairs instead of augmented image views. Language supervision endows CLIP features with information relating to the semantic meaning of image components, compared to models trained solely on image data [22]. We only use CLIP's image feature extractor in our experiments.
- **Stable Diffusion [77]:** Text-to-image diffusion models are an entirely different type of vision-language backbone, trained for image generation. The Stable Diffusion encoder, which we benchmark, maps images to a highly compressed latent space where diffusion is performed.
- **Random initialization:** In experiments where we fine-tune backbones on downstream tasks, we also evaluate baselines trained on the downstream training sets from random initialization.

B.3 The Pretraining Datasets

The backbones we benchmark are pretrained on datasets across a wide range of scales including image classification, image-text pairs, and images with depth annotations:

- **ImageNet-1k and -21k [17]:** ImageNet-21k contains over 14 million training images in 21,841 classes. ImageNet-1k is a subset of the aforementioned dataset containing almost 1.3 million training images in 1000 classes. These popular web-scraped image classification datasets are used for supervised pretraining with the labels, or self-supervised pretraining without them, among numerous backbones we benchmark. We denote pretraining on ImageNet-21k followed by fine-tuning on ImageNet-1k by "ImageNet-21k-1k".
- **LAION-2B [81]:** LAION-2B is a subset of the larger LAION-5B, which contains 5.85 billion web-scraped image-text pairs filtered by CLIP. LAION-2B specifically contains those 2.32 billion pairs with English language captions. Despite being by far the largest dataset amongst those we consider, LAION-2B is known to contain a large number of duplicates [97]. Stable Diffusion is further fine-tuned on LAION-Aesthetic, a subset of LAION-2B containing 120 million images filtered by a model trained to rate images by aesthetics.
- **CLIP [73]:** Since there is no OpenCLIP ResNet checkpoint available, we use the original CLIP checkpoint trained on OpenAI's diverse proprietary captioned-image dataset containing 400 million images scraped from publicly available internet sources.
- **MiDaS [75]:** MiDaS was trained on a combination of 12 image datasets with various types of depth annotations, and objectives: ReDWeb [101], DIML [42], Movies [75], MegaDepth [53], WSVD [92], TartanAir [96], HRWSI [102], ApolloScape [35], BlendedMVS [104], IRS [94], KITTI [62], NYU Depth V2 [82]. These models are therefore trained with multi-objective optimization. Collectively, the MiDaS training set contains more than 3.7 million images. An earlier version of MiDaS was trained on a smaller collection of 5 datasets, but we use the most recent version trained on the largest training set.

Evaluation datasets and licenses. In Table 4, Table 5, Table 6, and Table 7 we summarize the datasets we use for evaluating classification, object detection, segmentation, out-of-domain generalization and retrieval performance. We include the number of classes as well as the number of test samples for each dataset. To be noticed, we only use 10% of the labeled dataset for EuroSAT and Chexpert to distinguish the performance among all the backbones. Object detection and instance segmentation experiments are conducted on COCO dateset [54]. COCO is released under the Creative Commons Attribution 4.0 License[4]. This license permits users to share and adapt the dataset for any purpose, as long as the original creators are appropriately credited. For OOD classification, we use the ImageNet-Adversarial [34], ImageNet-Sketch [93], ImageNet-Renditions [33], ImageNet-V2 [76], and VisDA [66] datasets, all of which are freely available for research use. For OOD detection, we use the Sim10k [38] and Cityscapes [15] datasets. Densely annotated images for Sim10k are available freely[5] and can only be used for non-commercial applications. The license agreement for the Cityscapes dataset dictates that the dataset is made freely available to academic and non-academic entities for non-commercial purposes such as academic research, teaching, scientific publications, or personal experimentation and that permission to use the data is granted under certain

---

[4]https://cocodataset.org/#termsofuse
[5]https://fcav.engin.umich.edu/projects/driving-in-the-matrix

https://doi.org/10.52202/075280-1277

Table 4: **Image Classification Datasets**

Dataset	Description	Size	Classes
ImageNet-1k [17]	Natural images of versatile categories	1.3M	1,000
CIFAR-100 [46]	Natural images of versatile categories	50K	100
EuroSAT [31]	Satellite images (RGB) of land use and land cover	13.5K	10
Flowers-102 [65]	Images of flowers categories	1K	102
Aircraft [61]	Images of aircraft model variant, family, manufacturer	3K	100
Chexpert [37]	Medical images	191K	5

Table 5: **Object Detection and Instance Segmentation Datasets**

Dataset	Description	Size	Classes
COCO [54]	Large-scale object detection and segmentation dataset	330K	80

conditions.[6] All datasets used in benchmarking retrieval tasks (except for Objectnet) are restricted to non-commercial research and educational purposes. Objectnet is free to use for both research and commercial applications.[7]

C Experimental Details

C.1 Implementation Details

Classification. For **fine-tuning**, we train the backbones for 100 epochs using AdamW [60] and weight decay $\{5e^{-2}, 1e^{-3}\}$. We use a cosine annealing learning rate scheduler with 5 warmup epochs. We run grid searches for learning rates with the default grid range being $\{1e^{-3}, 5e^{-4}, 1e^{-4}\}$ as we observe peaking performance on multiple models with these learning rates. We expand the search range for learning rate when training models from scratch (*i.e.*, fine-tuning from randomly initialized weights) to $\{1e^{-2}, 5e^{-3}, 1e^{-3}, 5e^{-4}, 1e^{-4}\}$. We keep the batch size of 1024 the same for all experiments and use gradient accumulation when Out-of-Memory occurs for large models (such as the Stable Diffusion encoder). For data augmentation, we follow He et al. [30], including random horizontal flips and crops, mixup, CutMix, and a RandAug [16] policy with hyperparameter $(9, 0.5)$ corresponding to the number of transformations and magnitude. For regularization strategies, we apply the stochastic depths with a drop rate of 0.1, layer-wise learning rate decay of 0.75, and label smoothing with a rate of 0.1. For **linear probing**, again we follow He et al. [30], where we set weight decay to zero and disable Mix-Up, Cut-Mix, stochastic depth, or color jitter. We train the model with LARS optimizer with a batch size of 4096 for 90 epochs. For **fine-tuning on low-shot ImageNet**, we follow Cai et al. [6], where we use AdamW for all the transformer-based backbones and SGD for Convolution-only backbones. For transformer-based backbones, we use grid search among three peak learning rates of $\{1e^{-4}, 2.5e^{-4}, 5e^{-4}\}$ and two layer-decay rates of $0.65, 0.75$ for AdamW. We use grid search among three peak learning rates of $\{1e^{-1}, 5e^{-2}\}$ for SGD. We fix the

---

[6]https://www.cityscapes-dataset.com/license/
[7]https://objectnet.dev/download.html

Table 6: **OOD Generalization Datasets**

Task	Train Dataset	Test Dataset	Test Size	Classes
Image Classification	ImageNet-1K [79]	ImageNet-A [34]	7.5K	0.2K
Image Classification	ImageNet-1K [79]	ImageNet-v2 [76]	10K	1K
Image Classification	ImageNet-1K [79]	ImageNet-R [33]	30K	0.2K
Image Classification	ImageNet-1K [79]	ImageNet-S [93]	50K	1K
Image Classification	VisDA-Synthetic [66]	VisDA-Real [66]	55.4K	12
Object Detection	Sim10K [38]	Cityscapes [15]	0.5K	1

Table 7: **Image Retrieval Datasets**: Kindly note that the provided numbers are approximate references. For precise details, please consult the original research papers.

Dataset	Description	Size	Classes
CUB-200 [91]	Fine-grained bird images	12k	200
i-Naturalist [88]	Fine-grained species classification	450k	>1k
Object Net [2]	Object recognition dataset with uncommon poses	50k	313
INSTRE [95]	Fine-grained recognition data set of toys and house-hold objects	28k	200
Google Landmarks V2 [98]	Landmarks across the world	>1 mil	>1k
Oxford [69]	Specific buildings from Oxford	6400	12
Paris [70]	Specific landmarks and buildings from Paris	5000	11
Copy Days [19]	Copy detection dataset of landscapes, buildings etc	2,286	n/a

weight decay to be 0.05 and use the same data augmentation as the regular **fine-tuning** for 10% but without strong data augmentations, such as mix-up, cut-mix, and random erasing for the 1% setup.

Object Detection and Segmentation. For the training of Cascade Mask R-CNN, we adopt the standard training settings previously employed in ConvNext [58], Swin [56], and ViTDet [52]. For all experiments, we utilize the AdamW optimizer [60] with weight decay of 0.05, batch size of 16, and we conduct a grid search for the learning rate, considering values of $\{8e^{-5}, 1e^{-4}, 2e^{-4}, 3e^{-4}\}$. Additionally, we employ a $3\times$ schedule, spanning a total of 36 epochs, and the learning rate decayed by a factor of 10 at epochs 27 and 33. In addition, we apply multi-scale training [7, 83], excluding ViT-based backbones and Stable Diffusion. For ViT-based backbones, inspired by the approach employed in VITDet along with the fact that ViT backbones perform poorly on detection without specially tailored training strategies, we use *large-scale jitter* (LSJ) with the image resolution of 1024×1024 and scale range of $[0.1, 2.0]$. In order to maintain fair comparisons across backbones, we minimize architecture-specific modifications. Thus, for our ViT backbones, we avoid implementing some ViTDet modifications such as "simple feature pyramid" instead of FPN. Instead, we employ an FPN that utilizes the final feature map, without employing stage division. It is worth noting, as highlighted in the ViTDet paper, the performance of "FPN, last-map" is inferior to the "simple feature pyramid". Additionally, we use the supervised training results from DeiT [85] for supervised ViT-S and ViT-B pretrained backbones. For Stable Diffusion, we use a single resolution of 512×512 (resizing the image such that the longer side is 512) to overcome the significantly larger computational cost of this backbone compared to its competitors in our benchmark.

A note on ViTDet and scale: architectural modifications and very long training schedules can benefit ViTs in particular, as was found in Li et al. [52]. Similarly, Chen et al. [14] point out that ViTDet achieves stronger performance than their own work due to long and expensive training routines, behavior which stems from ViTs weak vision inductive bias. Additionally, in our analysis, we found that ViTs benefit more from scale, so ViTs might overtake other models at larger scales. Including large models in our benchmark, which includes many tasks and pretraining methods, would be prohibitively expensive, yet practitioners with sufficient computational resources for larger models, longer training routines, and architectural modifications may consider ViT backbones.

Syn-to-Real Generalization. For VisDA [66] Syn→Real, we report accuracy on the target domain (real) using models trained on the source domain (synthetic) for 12-way classification. For training, we use a learning rate of $1e^{-3}$ on 4 A40 GPUs with a batch size of 64 and report accuracy after 10 epochs. For object detection, we train the backbones outlined in Appendix B.1 with the Cascade-RCNN architecture. For training and fine-tuning backbones on Sim10k [38], we use a learning rate of $1e^{-4}$ on 4 A40 or RTX 6000 GPUs. To enable consistent evaluation across all backbones (CNNs and ViTs), we downsample Cityscapes [15] images to 1024×512 during evaluation. We train all models on the entirety of Sim10k and evaluate on the validation split of Cityscapes.

Image Retrieval. We have only evaluated pretrained models for this task. Dataset and metrics are discussed in the main body. Refer to table Table 7 for a brief summary of all the retrieval datasets.

D   Results

Image Classification. We present the ImageNet Top-1 and Top-5 classification accuracy for backbones pretrained with different methods and on various datasets in Table 8. We adopt the ImageNet results for supervised learning with random initialization from the `timm` library [100]. We omit

ImageNet results for ImageNet-pretrained backbones since those coincide with the randomly initialized backbones on ImageNet. We also present top-1 classification accuracy for finetuning on various datasets in Table 9, and we include ImageNet calibration and uncertainty estimation results in Table 10.

Table 8: **Classification accuracy (%) for ImageNet-related tasks.** "lp" denotes linear probing, "1%" and "10%" denote the percentage of labeled training images used during the fine-tuning.

Backbone	Method	Pretrain Data	ImageNet (lp)		ImageNet		ImageNet (10%)		ImageNet (1%)	
			Top-1	Top-5	Top-1	Top-5	Top-1	Top-5	Top-1	Top-5
ResNet-50	Supervised	ImageNet-1k	-	-	80.38	94.60	-	-	-	-
	VicReg	ImageNet-1k	72.15	90.22	78.77	94.29	69.54	89.07	55.04	79.34
	CLIP	LAION-2B	65.98	87.84	80.55	95.26	69.26	89.91	43.78	70.67
	DINO	ImageNet-1k	74.17	91.56	79.08	94.60	68.18	89.35	51.38	77.82
ViT-Small	Supervised	ImageNet-1k	-	-	78.84	94.29	-	-	-	-
	MoCoV3	ImageNet-1k	73.11	90.94	79.65	94.96	70.27	90.11	54.14	79.15
	DINO	ImageNet-1k	76.08	92.63	81.33	95.71	73.83	91.89	58.15	80.07
ViT-Base	Supervised	ImageNet-1k	-	-	79.15	94.09	-	-	-	-
	MoCoV3	ImageNet-1k	75.96	92.69	82.85	96.31	74.80	92.54	62.88	85.31
	MAE	ImageNet-1k	67.67	87.49	83.41	96.50	72.87	91.54	56.02	81.07
	DINO	ImageNet-1k	77.31	93.43	83.40	96.42	75.92	93.30	63.92	84.52
	CLIP	LAION-2B	79.74	95.53	85.19	97.46	78.67	95.00	66.44	89.11
SwinV2-Tiny	Supervised	ImageNet-1k	-	-	81.82	95.99	-	-	-	-
	MiDaS	MiDaS	76.44	92.66	82.55	95.92	79.92	94.57	75.44	90.83
SwinV2-Base	Supervised	ImageNet-21k-1k	-	-	87.10	98.23	-	-	-	-
	MiDaS	MiDaS	81.09	95.47	86.48	98.00	84.14	96.91	79.26	93.66
Stable Diffusion	Stable Diffusion	LAION-2B	-	-	79.90	95.10	71.50	89.07	38.02	65.78

Table 9: **Top-1 classification accuracy (%) for fine-tuning pretrained (and randomly initialized) backbones with different methods on various datasets.** We omit the ImageNet performance for the backbones trained on ImageNet in a supervised fashion that setup is the same as backbones trained from random initialization.

Backbone	Method	Pretrain Data	ImageNet	EuroSAT	Flower	CIFAR-100	Chexpert	Aircraft
ResNet-50	Rand Init	-	80.38	89.61	41.96	72.33	86.67	20.73
	Supervised	ImageNet-1k	-	98.26	86.52	84.71	86.82	55.31
	VicReg	ImageNet-1k	78.77	95.11	92.68	87.56	86.55	67.51
	CLIP	LAION-2B	80.55	98.72	90.62	84.35	88.92	73.50
	DINO	ImageNet-1k	79.08	98.74	94.04	86.49	87.49	74.13
ResNet-101	Rand Init	-	81.93	62.07	44.51	67.94	87.41	13.08
	Supervised	ImageNet-1k	-	97.19	83.59	83.07	86.51	40.47
ViT-Small	Rand Init	-	78.84	42.61	38.73	56.08	77.36	5.52
	Supervised	ImageNet-1k	-	95.54	96.17	89.48	87.60	61.69
	Supervised	ImageNet-21k	81.39	95.30	98.73	92.51	87.39	59.89
	MoCoV3	ImageNet-1k	79.65	96.02	83.59	89.38	88.10	54.68
	DINO	ImageNet-1k	81.33	89.09	73.73	90.00	87.75	48.20
ViT-Base	Rand Init	-	79.15	48.33	40.20	54.30	79.61	6.99
	Supervised	ImageNet-1k	-	96.22	94.04	90.62	87.27	62.02
	Supervised	ImageNet-21k	84.53	94.93	99.41	93.89	87.72	70.2
	MoCoV3	ImageNet-1k	82.85	96.74	94.53	90.89	86.82	71.55
	MAE	ImageNet-1k	83.41	95.54	94.63	89.96	88.01	72.27
	DINO	ImageNet-1k	83.40	95.59	97.17	91.22	87.05	71.82
	CLIP	LAION-2B	85.19	94.37	96.78	91.29	87.74	76.38
SwinV2-Tiny	Rand Init	-	81.82	89.33	29.90	66.49	87.76	5.31
	Supervised	ImageNet-1k	-	98.91	96.58	89.50	88.39	68.71
	MiDaS	MiDaS	82.55	96.33	96.48	90.53	87.69	69.54
SwinV2-Base	Supervised	ImageNet-21k-1k	87.10	95.94	99.61	93.09	87.73	79.46
	MiDaS	MiDaS	86.48	96.53	99.32	93.08	88.08	79.62
ConvNeXt-Tiny	Rand Init	-	82.10	73.80	18.24	75.31	83.25	4.35
	Supervised	ImageNet-1k	-	95.70	96.00	89.89	87.56	69.99
ConvNeXt-Base	Rand Init	-	83.88	30.39	19.41	73.04	85.26	4.02
	Supervised	ImageNet-1k	-	93.06	94.92	88.98	88.98	64.72
	Supervised	ImageNet-21k	85.87	96.19	99.61	92.84	87.80	69.39
Stable Diffusion	Stable Diffusion	LAION-2B	79.90	92.22	91.89	90.50	87.49	72.45

Object Detection and Segmentation. In our experiment, we utilize the *train2017* and *val2017* splits of the COCO dataset for training and evaluation, respectively. We report results on bounding box object detection (AP^{box}) and instance segmentation (AP^{mask}). In Table 11, Table 12 and Table 13, we present the comprehensive results of our experiment. Table 11 reflects the results obtained with various backbone architectures when the detector is fine-tuned while the backbone remains frozen. Table 12 contains both training from scratch with randomly initialized backbones as well as end-to-end fine-tuning using pretrained backbones. In Table 13, we additionally present results on the harder

Table 10: **Calibration and uncertainty estimation on ImageNet.** We measure Top-1 accuracy (%), cross-entropy test loss (**CE**), and expected calibration error (**ECE**).

Backbone	Method	Pretrain Data	Accuracy	CE	ECE
ResNet-50	Supervised	ImageNet-1k	80.38	0.94	0.09
	VicReg	ImageNet-1k	78.77	1.11	0.21
	CLIP	LAION-2B	80.55	1.02	0.19
	DINO	ImageNet-1k	79.08	1.11	0.22
ResNet-101	Supervised	ImageNet-1k	81.93	0.92	0.16
ViT-Small	Supervised	ImageNet-1k	78.84	0.84	0.03
	Supervised	ImageNet-21k	81.39	0.68	0.01
	MoCoV3	ImageNet-1k	79.65	0.90	0.11
	DINO	ImageNet-1k	81.33	0.83	0.10
ViT-Base	Supervised	ImageNet-1k	79.15	0.86	0.05
	Supervised	ImageNet-21k	84.53	0.56	0.01
	MoCoV3	ImageNet-1k	82.85	0.77	0.08
	MAE	ImageNet-1k	83.41	0.75	0.09
	DINO	ImageNet-1k	83.40	0.76	0.07
	CLIP	LAION-2B	85.19	0.66	0.08
SwinV2-Tiny	Supervised	ImageNet-1k	81.82	0.83	0.09
	MiDaS	MiDaS	82.55	0.83	0.07
ConvNeXt-Tiny	Supervised	ImageNet-1k	82.10	0.79	0.06
ConvNeXt-Base	Supervised	ImageNet-1k	83.88	0.69	0.04
	Supervised	ImageNet-21k	85.87	0.56	0.03

LVIS dataset [27] using the best transformer-based (SwinV2) and convolutional-based (ConvNeXt) architectures from our experiments at several sizes. We again see a benefit of scale here as well as the slightly superior performance of modern convolutional architectures. These tables provide a comprehensive overview of the performance achieved across various backbones and scenarios, enabling a thorough analysis and comparison of the different backbones utilized in our study.

Table 11: **Object detection and instance segmentation using Cascade Mask-RCNN on COCO with frozen backbones.**

Backbone	Method	Pretrain Data	Params	Input Size	AP^{box}	AP^{box}_{50}	AP^{box}_{75}	AP^{mask}	AP^{mask}_{50}	AP^{mask}_{75}
ResNet-50	Supervised	ImageNet-1k	82M	1333 × 800	42.5	61.0	46.2	37.1	58.1	39.5
	VicReg	ImageNet-1k	82M	1333 × 800	44.1	62.3	48.1	38.8	59.7	42.0
	DINO	ImageNet-1k	82M	1333 × 800	44.6	62.9	48.8	39.0	60.3	42.0
ResNet-101	Supervised	ImageNet-1k	101M	1333 × 800	43.4	62.1	47.1	38.0	59.3	40.7
ViT-Small	Supervised	ImageNet-1k	84M	1024 × 1024	27.3	44.3	29.1	23.6	40.8	23.9
	MoCoV3	ImageNet-1k	84M	1024 × 1024	27.8	44.6	29.7	24.2	41.5	24.9
	DINO	ImageNet-1k	84M	1024 × 1024	33.6	52.5	35.9	29.1	49.0	30.0
ViT-Base	Supervised	ImageNet-1k	155M	1024 × 1024	34.1	54.0	36.1	29.6	50.6	30.0
	MoCoV3	ImageNet-1k	155M	1024 × 1024	32.1	50.4	34.6	28.2	47.1	29.3
	MAE	ImageNet-1k	155M	1024 × 1024	35.6	54.0	38.7	31.8	51.1	33.7
	DINO	ImageNet-1k	155M	1024 × 1024	36.2	55.6	39.1	31.7	52.2	32.9
	CLIP	LAION-2B	155M	1024 × 1024	21.9	36.7	22.5	18.8	33.6	18.8
SwinV2-Tiny	Supervised	ImageNet-1k	86M	1333 × 800	36.9	55.4	39.9	32.5	52.6	34.4
	MiDaS	MiDaS	86M	1333 × 800	34.3	51.5	37.2	30.2	48.9	32.0
SwinV2-Base-w8	Supervised	ImageNet-1k	145M	1333 × 800	38.6	57.4	41.7	33.5	54.4	35.3
SwinV2-Base-w24	Supervised	ImageNet-21k-1k	145M	1333 × 800	44.6	64.7	48.6	38.8	61.6	41.5
	MiDaS	MiDaS	145M	1333 × 800	42.2	61.5	45.9	37.1	58.7	39.3
ConvNeXt-Tiny	Supervised	ImageNet-1k	86M	1333 × 800	44.4	63.1	48.7	38.7	60.7	41.6
ConvNeXt-Base	Supervised	ImageNet-1k	146M	1333 × 800	44.8	64.1	48.6	39.2	61.4	42.0
	Supervised	ImageNet-21k	146M	1333 × 800	46.2	66.0	50.2	40.1	62.9	43.0
Stable Diffusion	Stable Diffusion	LAION-2B	442M	1333 × 800	38.2	55.4	41.6	34.0	52.7	36.4

https://doi.org/10.52202/075280-1277

Table 12: **Object detection and instance segmentation results using Cascade Mask-RCNN on COCO.**

Backbone	Method	Pretrain Data	Params	Input Size	AP^{box}	AP^{box}_{50}	AP^{box}_{75}	AP^{mask}	AP^{mask}_{50}	AP^{mask}_{75}
ResNet-50	Random Init	-	82M	1333×800	41.3	57.4	45.1	36.0	55.1	38.9
	Supervised	ImageNet-1k	82M	1333×800	46.6	64.6	50.6	40.2	61.9	43.5
	VicReg	ImageNet-1k	82M	1333×800	38.2	55.2	41.5	33.5	52.9	35.9
	DINO	ImageNet-1k	82M	1333×800	45.4	63.5	49.2	39.4	61.1	42.4
ResNet-101	Random Init	-	101M	1333×800	45.7	63.0	50.0	39.5	60.5	43.1
	Supervised	ImageNet-1k	101M	1333×800	47.7	65.6	52.0	41.3	63.2	44.6
ViT-Small	Random Init	-	84M	1024×1024	43.2	62.2	47.2	38.0	59.3	40.7
	Supervised	ImageNet-1k	84M	1024×1024	48.2	68.1	51.8	41.7	65.0	44.7
	MoCoV3	ImageNet-1k	84M	1024×1024	47.6	67.5	51.7	41.6	64.3	44.4
	DINO	ImageNet-1k	84M	1024×1024	48.2	67.6	52.4	42.3	64.9	44.9
ViT-Base	Random Init	-	155M	1024×1024	46.0	65.0	50.7	40.1	62.3	43.1
	Supervised	ImageNet-1k	155M	1024×1024	49.4	69.3	53.5	42.9	66.1	46.2
	MoCoV3	ImageNet-1k	155M	1024×1024	49.7	69.4	53.9	43.2	66.6	46.5
	MAE	ImageNet-1k	155M	1024×1024	51.3	70.3	55.9	44.5	67.7	48.1
	DINO	ImageNet-1k	155M	1024×1024	49.5	69.0	53.7	42.8	66.1	46.0
	CLIP	LAION-2B	155M	1024×1024	50.0	69.3	54.4	43.3	66.3	46.6
SwinV2-Tiny	Random Init	-	86M	1333×800	47.0	65.3	51.2	40.8	62.7	44.1
	Supervised	ImageNet-1k	86M	1333×800	50.2	69.1	54.6	43.4	66.3	46.9
	MiDaS	MiDaS	86M	1333×800	50.2	69.3	54.5	43.5	66.4	47.0
SwinV2-Base-w8	Random Init	-	145M	1333×800	48.1	66.6	52.3	41.5	64.1	44.7
	Supervised	ImageNet-1k	145M	1333×800	52.4	71.0	57.1	45.2	68.6	49.1
SwinV2-Base-w24	Supervised	ImageNet-21k-1k	145M	1333×800	52.9	71.4	57.5	45.7	69.0	49.6
	MiDaS	MiDaS	145M	1333×800	52.7	71.4	57.2	45.7	69.0	49.7
ConvNeXt-Tiny	Random Init	-	86M	1333×800	47.5	65.5	51.7	41.2	63.0	44.3
	Supervised	ImageNet-1k	86M	1333×800	49.9	68.4	54.3	43.2	66.0	46.8
ConvNeXt-Base	Random Init	-	146M	1333×800	48.3	66.4	52.7	41.9	63.8	45.3
	Supervised	ImageNet-1k	146M	1333×800	51.7	70.2	56.0	44.6	67.7	48.3
	Supervised	ImageNet-21k	146M	1333×800	52.9	71.7	57.3	45.8	69.2	49.9
Stable Diffusion	Random Init	-	442M	1333×800	37.1	51.4	40.1	31.9	43.7	31.2
	Stable Diffusion	LAION-2B	442M	1333×800	43.4	59.1	46.3	38.1	56.9	40.2

Table 13: **Object detection and instance segmentation using Cascade Mask-RCNN on LVIS v1.**

Backbone	Method	Pretrain Data	Params	Input Size	AP^{box}	AP^{box}_{50}	AP^{box}_{75}	AP^{mask}	AP^{mask}_{50}	AP^{mask}_{75}
SwinV2-Tiny	Supervised	ImageNet-1k	86M	1333×800	33.0	46.3	35.3	29.9	44.5	31.9
	MiDaS	MiDaS	86M	1333×800	32.6	45.7	34.9	29.6	43.9	32.0
SwinV2-Base-w8	Supervised	ImageNet-1k	145M	1333×800	35.7	48.7	38.0	32.0	47.0	34.4
ConvNeXt-Tiny	Supervised	ImageNet-1k	86M	1333×800	33.2	46.1	35.4	29.9	44.3	32.2
ConvNeXt-Base	Supervised	ImageNet-1k	146M	1333×800	35.8	48.8	38.0	32.0	46.9	34.5

OOD Generalization. We include results for OOD generalization for image classification in Table 14 and for object detection in Table 15.

Table 14: **Top-1 OOD classification accuracy** (%).

Backbone	Method	Pretrain Data	Test Dataset				Train Dataset	Test Dataset
			ImageNet-A	ImageNet-S	ImageNet-R	ImageNet-V2		VisDA (real)
ResNet-50	Rand Init	-	-	-	-	-	VisDA (syn)	22.07
	Supervised	ImageNet-1k	10.03	29.63	40.25	68.75	VisDA (syn)	47.77
	VicReg	ImageNet-1k	10.29	28.63	39.98	67.56	VisDA (syn)	44.19
	CLIP	LAION-2B	15.53	30.10	42.44	69	VisDA (syn)	21.98
	DINO	ImageNet-1k	10.13	28.38	39.74	67.55	VisDA (syn)	-
ResNet-101	Rand Init	-	-	-	-	-	VisDA (syn)	21.81
	Supervised	ImageNet-1k	19.04	34.73	45.10	70.88	VisDA (syn)	56.56
ViT-Base	Rand Init	-	-	-	-	-	VisDA (syn)	22.16
	Supervised	ImageNet-1k	14.85	27.99	38.02	66.45	VisDA (syn)	63.57
	Supervised	ImageNet-21k-1k	43.24	43.21	56.79	74.01	VisDA (syn)	65.62
	MoCoV3	ImageNet-1k	32.57	37.33	34.85	72.71	VisDA (syn)	57.21
	MAE	ImageNet-1k	36.2	34.75	48.77	73.47	VisDA (syn)	48.90
	DINO	ImageNet-1k	35.32	36.52	49.15	72.71	VisDA (syn)	59.96
	CLIP	LAION-2B	46.59	63.33	50.17	75.39	VisDA (syn)	46.05
SwinV2-Tiny	MiDaS	MiDaS	30.87	29.41	41.26	71.27	VisDA (syn)	61.62
SwinV2-Base	Supervised	ImageNet-21k-1k	45.97	37.00	49.69	74.42	VisDA (syn)	68.84
	MiDaS	MiDaS	63.05	48.77	63.12	77.06	VisDA (syn)	68.66
ConvNeXt-Base	Supervised	ImageNet-1k	41.92	37.29	51.07	74.09	VisDA (syn)	71.12
	Supervised	ImageNet-21k	60.8	48.92	62.53	76.96	VisDA (syn)	74.96

Table 15: **OOD object detection on Sim10k→Cityscapes.** Out-of-distribution generalization across backbones for object detection (Cascade-RCNN) models trained on Sim10k and evaluated on Cityscapes to detect instances of "car". (Frozen) column corresponds to settings where the backbone has been frozen.

Backbone	Method	Pretrain Data	mAP@50	mAP@50 (Frozen)
ResNet-50	Random Init	–	30.6	–
	Supervised	ImageNet-1k	46.5	52.4
	VicReg	ImageNet-1k	44.4	49.8
	DINO	ImageNet-1k	50.0	52.2
ResNet-101	Random Init	–	25.2	–
	Supervised	ImageNet-1k	46.9	52.6
ViT-Small	Random Init	–	8.7	–
	Supervised	ImageNet-1k	33.7	15.9
	MoCoV3	ImageNet-1k	32.8	19.4
	DINO	ImageNet-1k	43.0	31.3
ViT-Base	Random Init	–	10.3	–
	Supervised	ImageNet-1k	38.2	24.6
	MoCoV3	ImageNet-1k	36.7	27.9
	MAE	ImageNet-1k	44.2	32.3
	DINO	ImageNet-1k	41.7	35.1
	CLIP	LAION-2B	38.1	9.7
SwinV2-Tiny	Random Init	–	40.9	–
	Supervised	ImageNet-1k	48.0	48.2
	MiDaS	MiDaS	49.5	45.5
SwinV2-Base-w8	Random Init	–	38.0	–
	Supervised	ImageNet-1k	51.1	49.3
SwinV2-Base-w24	Supervised	ImageNet-21k-1k	51.0	50.2
	MiDaS	MiDas	52.5	50.3
ConvNeXt-Tiny	Random Init	–	36.2	–
	Supervised	ImageNet-1k	54.5	50.3
ConvNeXt-Base	Random Init	–	25.5	–
	Supervised	ImageNet-1k	55.5	52.1
	Supervised	ImageNet-21k	52.4	53.9

Retrieval. We present the mAP, MRR and Recall@5 values for various backbones across different datasets in Table 16, Table 17, and Table 18, respectively.

Analysis. In Table 20, we compare the performance of backbones pretrained with SSL (including CLIP) and supervised learning on ImageNet-1k and ImageNet-21k. We pick the top-3 backbones in each category and calculate the mean z-scores for all the tasks.

Adversarial robustness. In Table 19, we show adversarial robustness on the ImageNet test set against an untargeted PGD adversarial attack ϵ with ℓ_∞ constraints of $\frac{1}{255}$ and $\frac{2}{255}$. For attack hyperparameters, we use 20 steps and step size $\frac{\epsilon}{5}$.

E   Assets and Licenses

The assets used in this work can be categorized as – Code Repositories, Backbones and Dependencies (licenses for datasets are included in Appendix B.3).

Table 16: **MAP scores for image retrieval experiments.**

Backbone	Method	Pretrain Data	CUB	iNat	Obj	INSTRE	GLM	rOxf	rPar	CopyD
ConvNext-Base	Supervised	ImageNet-1k	20.55	5.53	11.42	52.13	12.71	26.73	55.84	79.32
	Supervised	ImageNet-21k-1k	62.51	19.43	19.57	69.4	21.34	42.42	73.33	86.18
ConvNext-Small	Supervised	ImageNet-1k	23.96	5.66	10.35	49.33	12.6	28.1	56.03	77.86
	Supervised	ImageNet-21k-1k	61.09	17.06	17.12	62.79	19.53	42.19	71.03	83.56
ConvNext-XLarge	Supervised	ImageNet-21k-1k	65.31	21.98	21.37	69.28	21.67	45.33	74.76	86.81
ResNet-101	CLIP	OpenAI	21.75	4.50	5.4	56.71	15.35	23.93	52.1	79.07
	Supervised	ImageNet-1k	22.86	5.52	8.9	47.37	13.83	31.27	58.51	78.52
ResNet-50	CLIP	OpenAI	15.37	3.45	3.81	48.10	14.20	24.09	52.14	79.61
	Supervised	ImageNet-1k	18.75	4.28	5.31	41.59	11.98	25.59	52.37	79.78
ResNet-50	VicReg	ImageNet-1k	8.84	3.15	1.82	42.45	13.76	31.71	58.24	82.48
ResNet-50x64	CLIP	OpenAI	42.30	10.02	15.11	85.38	26.91	41.93	70.27	91.36
SwinV2-Base	MiDaS	MiDaS	10.44	3.84	1.93	24.91	11.52	29.76	56.34	84.03
	Supervised	ImageNet-21k-1k	57.57	17.95	17.81	66.87	20.33	44.35	71.28	87.57
SwinV2-Base-w16	Supervised	ImageNet-21k-1k	58.77	19.93	18.6	69.48	20.97	44.91	71.7	88.2
SwinV2-Large-w16	Supervised	ImageNet-21k-1k	57.55	17.74	16.36	71	21.64	44.26	75.58	88.59
SwinV2-Tiny	MiDaS	MiDaS	10.44	3.84	1.93	24.91	11.52	29.76	56.34	84.03
SwinV2-Tiny	Supervised	ImageNet-1k	22.91	5.71	6.94	54.31	13.76	27.35	56.29	82.93
	Supervised	ImageNet-1k	22.91	5.71	6.94	54.31	13.76	27.35	56.29	82.93
ViT-Base	CLIP	LAION-2B	40.27	8.17	12.98	81.13	23.83	44.84	73.62	88.79
	MAE	ImageNet-1k	1.26	0.22	0.43	4.86	1.43	5.19	11.12	48.12
ViT-Base	MoCoV3	ImageNet-1k	12.97	4.16	2.29	40.53	12.11	30.25	51.6	84.75
	Supervised	ImageNet-1k	17.09	3.81	4.59	39.75	9.64	21.97	50.03	77.7
ViT-Base	Supervised	ImageNet-21k-1k	52.18	11.99	7.56	46.58	14.3	30.96	59.82	83.65
	DINO	ImageNet-1k	22.21	7.43	4.57	53.01	15.35	37.03	62.22	86.18
ViT-Large	CLIP	LAION-2B	47.77	9.62	12.87	80.29	25.45	39.19	70	90.32
	MAE	ImageNet-1k	2.53	0.84	0.53	12.24	3.78	13.26	24.92	70.34
ViT-Large	Supervised	ImageNet-21k-1k	62.44	18.19	16	55.18	18.49	37.68	67.07	87.04
Vit-Small	MoCoV3	ImageNet-1k	12.99	3.7	1.86	35.28	11.39	24.83	50.24	82.67
	Supervised	ImageNet-1k	19.44	4.05	4.61	40.45	10.51	21.69	49.08	79.54
Vit-Small	Supervised	ImageNet-21k-1k	49.6	10.22	6.34	48.17	14.37	31.24	61.5	81.92
	DINO	ImageNet-1k	31.38	7.35	3.99	52.64	14.79	37.98	61.01	85.3

Code Repositories. We provide supporting code for all our experiments here. For image classification experiments, we build on top of the `timm` library [100][8], the original MAE repo[9] and the medical dataset pretrain repo [103][10]. `timm` is distributed under Apache 2.0 License and MAE under the Attribution-NonCommercial 4.0 International License. For object detection, instance segmentation, and OOD detection experiments, we build on top of the MMDetection framework [9][11]. MMDetection is distributed under Apache License 2.0.

Backbones. We use publicly available pretrained backbones. The full list is provided in Appendix B.

Dependencies. Key dependencies for all our experiments include `pytorch`, `timm`, HuggingFace utilities and MMCV. Please see our repo README for a comprehensive list of all dependencies to reproduce the experiments.

F   Observations about Hyperparameters

For hyperparameter tuning, we find that the learning rate strategy is highly method- and dataset-dependent. For example, on ImageNet classification, the best learning rate we tried for CLIP was 1e-4 while the best learning rate for MAE was 1e-3, which is similar to the best learning fate for training from scratch. We speculate that this learning rate sensitivity occurs because different pretraining algorithms lead to parameter vectors of very different magnitudes. For image classification, a shorter

---

[8]https://github.com/huggingface/pytorch-image-models
[9]https://github.com/facebookresearch/mae
[10]https://github.com/lambert-x/Medical_MAE
[11]https://github.com/open-mmlab/mmdetection

Table 17: **MRR scores for image retrieval experiments.**

Backbone	Method	Pretrain Data	CUB	iNat	Obj	INSTRE	GLM	rOxf	rPar	CopyD
ConvNext-Base	Supervised	ImageNet-1k	0.63	0.15	0.38	0.88	0.37	0.63	0.97	0.87
	Supervised	ImageNet-21k-1k	0.9	0.41	0.52	0.94	0.53	0.84	0.99	0.92
ConvNext-Small	Supervised	ImageNet-1k	0.66	0.16	0.38	0.87	0.36	0.68	0.97	0.86
	Supervised	ImageNet-21k-1k	0.9	0.38	0.49	0.92	0.49	0.85	0.98	0.9
ConvNext-XLarge	Supervised	ImageNet-21k-1k	0.9	0.43	0.53	0.93	0.52	0.87	0.99	0.92
ResNet-101	CLIP	OpenAI	0.67	0.15	0.31	0.93	0.44	0.65	0.97	0.86
	Supervised	ImageNet-1k	0.66	0.16	0.35	0.86	0.4	0.67	0.97	0.86
ResNet-50	CLIP	OpenAI	0.59	0.12	0.24	0.88	0.41	0.67	0.97	0.86
	Supervised	ImageNet-1k	0.6	0.13	0.28	0.84	0.37	0.65	0.97	0.87
	VicReg	ImageNet-1k	0.45	0.11	0.18	0.86	0.42	0.8	0.97	0.89
ResNet-50x64	CLIP	OpenAI	0.83	0.27	0.53	0.99	0.60	0.85	0.99	0.95
SwinV2-Base	MiDaS	MiDaS	0.54	0.13	0.17	0.70	0.36	0.72	0.97	0.90
SwinV2-Base-w16	Supervised	ImageNet-21k-1k	0.89	0.4	0.51	0.93	0.51	0.87	0.99	0.92
SwinV2-Base-w24	Supervised	ImageNet-21k-1k	0.89	0.43	0.51	0.94	0.52	0.87	0.99	0.93
SwinV2-Large-w16	Supervised	ImageNet-21k-1k	0.88	0.39	0.47	0.94	0.52	0.84	0.98	0.93
SwinV2-Large-w24	Supervised	ImageNet-21k-1k	0.88	0.42	0.49	0.94	0.52	0.84	0.98	0.94
SwinV2-Tiny	MiDaS	MiDaS	0.51	0.09	0.16	0.64	0.35	0.58	0.96	0.88
	Supervised	ImageNet-1k	0.68	0.17	0.32	0.9	0.4	0.67	0.99	0.89
ViT-Base	CLIP	LAION-2B	0.82	0.23	0.46	0.98	0.55	0.87	0.97	0.93
	MAE	ImageNet-1k	0.14	0.01	0.04	0.34	0.07	0.33	0.81	0.61
	MoCoV3	ImageNet-1k	0.57	0.13	0.2	0.84	0.38	0.78	0.95	0.91
	Supervised	ImageNet-1k	0.56	0.12	0.23	0.84	0.3	0.56	0.95	0.86
	Supervised	ImageNet-21k-1k	0.85	0.29	0.33	0.88	0.41	0.74	0.96	0.9
	DINO	ImageNet-1k	0.72	0.21	0.29	0.91	0.43	0.85	0.99	0.91
ViT-Large	MAE	ImageNet-1k	0.24	0.04	0.05	0.56	0.16	0.53	0.92	0.81
	CLIP	LAION-2B	0.85	0.26	0.47	0.98	0.58	0.82	0.97	0.94
	Supervised	ImageNet-21k-1k	0.88	0.38	0.47	0.9	0.47	0.83	0.97	0.92
ViT-Small	MoCoV3	ImageNet-1k	0.57	0.12	0.18	0.82	0.36	0.7	0.97	0.89
	Supervised	ImageNet-1k	0.61	0.13	0.25	0.85	0.32	0.61	0.95	0.87
	Supervised	ImageNet-21k-1k	0.84	0.27	0.3	0.88	0.43	0.74	0.96	0.88
	DINO	ImageNet-1k	0.79	0.21	0.27	0.9	0.42	0.87	0.99	0.9

training period is enough for finetuning, where we only train the model for 100 epochs which is 1/3 as many epochs as we use for training from scratch. Also on smaller datasets, such as Flowers-102 and aircraft datasets, finetuning obtains much higher accuracy compared to training from scratch. In contrast, finetuning does not save quite as many epochs for detection and segmentation where detection systems contain lots of new parameters that are randomly initialized for downstream training.

Table 18: **Recall@5 scores for image retrieval experiments.**

Backbone	Method	Pretrain Data	CUB	iNat	Obj	INSTRE	GLM	rOxf	rPar	CopyD
ConvNext-Base	Supervised	ImageNet-1k	0.045	0.069	0.03	0.097	0.099	0.087	0.026	0.854
	Supervised	ImageNet-21k-1k	0.085	0.221	0.046	0.111	0.163	0.174	0.027	0.902
ConvNext-Small	Supervised	ImageNet-1k	0.05	0.069	0.029	0.094	0.099	0.092	0.026	0.851
	Supervised	ImageNet-21k-1k	0.084	0.196	0.042	0.106	0.151	0.169	0.027	0.888
ConvNext-XLarge	Supervised	ImageNet-21k-1k	0.086	0.247	0.048	0.111	0.164	0.172	0.027	0.903
ResNet-101	CLIP	OpenAI	0.05	0.06	0.02	0.106	0.117	0.082	0.026	0.848
	Supervised	ImageNet-1k	0.049	0.07	0.026	0.092	0.107	0.085	0.026	0.857
ResNet-50	CLIP	OpenAI	0.04	0.046	0.015	0.097	0.107	0.092	0.026	0.852
	Supervised	ImageNet-1k	0.043	0.056	0.018	0.089	0.099	0.084	0.026	0.836
	VicReg	ImageNet-1k	0.026	0.042	0.009	0.09	0.116	0.106	0.027	0.868
ResNet-50x64	CLIP	OpenAI	0.073	0.124	0.044	0.122	0.191	0.181	0.027	0.948
SwinV2-Base	MiDaS	MiDaS	0.032	0.051	0.008	0.063	0.095	0.113	0.027	0.890
SwinV2-Base-w16	Supervised	ImageNet-21k-1k	0.083	0.207	0.043	0.109	0.154	0.178	0.027	0.917
SwinV2-Base-w24	Supervised	ImageNet-21k-1k	0.084	0.226	0.045	0.111	0.158	0.177	0.027	0.923
SwinV2-Large-w16	Supervised	ImageNet-21k-1k	0.082	0.204	0.04	0.112	0.16	0.167	0.027	0.93
SwinV2-Large-w24	Supervised	ImageNet-21k-1k	0.083	0.223	0.041	0.113	0.161	0.17	0.027	0.931
SwinV2-Tiny	MiDaS	MiDaS	0.031	0.034	0.008	0.055	0.095	0.059	0.026	0.849
	Supervised	ImageNet-1k	0.052	0.072	0.021	0.101	0.114	0.096	0.027	0.868
ViT-Base	CLIP	LAION-2B	0.071	0.104	0.037	0.12	0.172	0.175	0.027	0.92
	MAE	ImageNet-1k	0.005	0.003	0.001	0.02	0.012	0.02	0.015	0.542
	MoCoV3	ImageNet-1k	0.036	0.055	0.01	0.088	0.1	0.114	0.026	0.887
	Supervised	ImageNet-1k	0.039	0.049	0.015	0.088	0.078	0.053	0.025	0.82
	Supervised	ImageNet-21k-1k	0.077	0.146	0.024	0.094	0.111	0.088	0.026	0.883
	DINO	ImageNet-1k	0.055	0.093	0.018	0.102	0.125	0.158	0.027	0.894
ViT-Large	CLIP	LAION-2B	0.077	0.122	0.038	0.12	0.183	0.127	0.027	0.934
	MAE	ImageNet-1k	0.01	0.012	0.002	0.042	0.036	0.038	0.023	0.753
	Supervised	ImageNet-21k-1k	0.082	0.207	0.04	0.099	0.141	0.15	0.027	0.9
Vit-Small	MoCoV3	ImageNet-1k	0.037	0.05	0.009	0.082	0.097	0.094	0.026	0.877
	Supervised	ImageNet-1k	0.044	0.053	0.016	0.088	0.085	0.062	0.025	0.843
	Supervised	ImageNet-21k-1k	0.076	0.126	0.021	0.097	0.118	0.097	0.026	0.869
	DINO	ImageNet-1k	0.065	0.093	0.016	0.101	0.123	0.16	0.027	0.888

Table 19: **Top-1 classification accuracy (%) for ImageNet against adversarial attacks with ℓ_∞ constraint radii** $1/255$ **and** $2/255$**.**

Backbone	Method	Pretrain Data	Clean	$\epsilon = 1/255$	$\epsilon = 2/255$	Z-scores
ResNet-50	Supervised	ImageNet-1k	80.38	28.79	13.25	-0.99
	VicReg	ImageNet-1k	78.77	36.60	22.01	-0.26
	CLIP	LAION-2B	80.55	32.78	18.55	0.58
	DINO	ImageNet-1k	79.08	35.80	20.75	-0.35
ResNet-101	Supervised	ImageNet-1k	81.93	44.23	32.43	0.53
ViT-Small	Supervised	ImageNet-1k	78.84	21.21	6.42	-1.62
	Supervised	ImageNet-21k	81.39	16.50	3.83	-1.94
	MoCoV3	ImageNet-1k	79.65	48.62	32.16	0.71
	DINO	ImageNet-1k	81.33	47.87	30.04	0.57
ViT-Base	Supervised	ImageNet-1k	79.15	27.08	9.54	-1.23
	Supervised	ImageNet-21k	84.53	23.04	6.92	-1.52
	MoCoV3	ImageNet-1k	82.85	55.44	39.49	1.32
	MAE	ImageNet-1k	83.41	50.85	31.69	0.77
	DINO	ImageNet-1k	83.40	53.59	36.61	1.11
	CLIP	LAION-2B	85.19	47.91	28.35	0.50
SwinV2-Tiny	Supervised	ImageNet-1k	81.82	40.91	23.15	-0.03
	MiDaS	MiDaS	82.55	41.44	25.20	0.08
ConvNeXt-Tiny	Supervised	ImageNet-1k	82.10	49.74	31.42	0.72
ConvNeXt-Base	Supervised	ImageNet-1k	83.88	55.31	37.19	1.21
	Supervised	ImageNet-21k	85.87	53.78	34.05	1.00

Table 20: **Z-scores for best-performing SSL and supervised learning backbones.** Mean z-scores for each task averaged across the 3 top performing backbones dividing models into self (weakly-)-supervised learning (SSL) on ImageNet-1k, supervised learning on ImageNet-1k (Sup-1k), and ImageNet-21k (Sup-21k).

Task	SSL	Sup-1k	Sup-21k
Cls	0.573	0.527	0.936
Det	0.298	0.743	1.076
Seg	0.314	0.717	1.071
Ret	0.489	-0.079	0.708
(OOD) Cls	0.419	0.287	1.271
(OOD) Det	0.414	0.923	0.853